



On the seasonal and inter-annual variability of the equatorial Indian Ocean surface winds

C. Shaji¹ · S. Ruma¹

Received: 17 February 2018 / Accepted: 15 August 2019 / Published online: 11 September 2019
© Springer-Verlag GmbH Austria, part of Springer Nature 2019

Abstract

Variability of the Equatorial Indian Ocean (EIO) winds play crucial roles in driving the upper EIO dynamics and modifying the ocean–atmosphere interactions in the Indian Ocean (IO). This study, using a satellite-sensed high-resolution ($0.25^\circ \times 0.25^\circ$) monthly winds, has revealed many salient features of the seasonal and inter-annual variability of winds at various dynamically significant regions of the EIO. Though annual mean wind pattern of the EIO shows westerlies east of 60°E , the different local areas in this ocean exhibit significant seasonal wind variations. Migrations and fluctuations of southerlies and westerlies primarily determine the EIO wind variability. In the western (eastern) EIO, SW and NE monsoon winds are stronger (weaker) and of longer (shorter) duration. Near to the equator (1°S – 1°N), in the central EIO, weaker winds occur during SW and NE monsoons, whereas stronger winds during transition periods. Near the equator, meridional winds show a significant annual period, especially in the western EIO. But zonal winds exhibit semi-annual period east of 55°E with a peak in the central ocean associated with the active westerlies during spring and fall, and annual period west of 55°E in the western EIO due to monsoon reversals. Westerlies are stronger during the fall compared to spring. Zonal wind variability in the central EIO is the essential deciding factor for the zonal wind variability occurring in the whole EIO. Both Zonal Sea Level Pressure Gradient (ZSLPG) and Momentum Advection (MA) fields determine the dynamics of zonal winds in the EIO. Zonal winds are weak in the western EIO because of the semi-annual harmonics of both ZSLPG and MA, though with substantial amplitude, exhibiting opposite accelerations there. But stronger zonal winds occur in the central EIO (60°E – 80°E) because of the same accelerations set by the relatively weaker ZSLPG and MA fields. The zonal winds show substantial inter-annual variability compared to the meridional winds. The inter-annual variability of zonal winds shows the predominance of two modes, with EOF1 50% and EOF2 20% of the total variance. Zonal wind pattern of EOF1 resembles the monsoon transition seasons, while that of EOF2 describes the SW monsoon. In the EIO, Indian Ocean Dipole (IOD) influences the patterns of winds and SST anomalies better than that of El Niño–Southern Oscillation (ENSO). Spatiotemporal variability of the EIO winds during ENSO and IOD indicates the prevalence of stronger zonal wind anomalies in the eastern and central EIO and weaker anomalies in the western EIO. Although spatial patterns of wind anomalies are similar during El Niño and Positive IOD (PIOD) periods, the monthly variations, spatial extensions, and intensities of anomalies are much different while comparing. Prospectus for understanding the EIO winds variations can help to understand the changes occurring in the wind-driven surface and subsurface zonal currents.

Communicated by S. Trini Castelli.

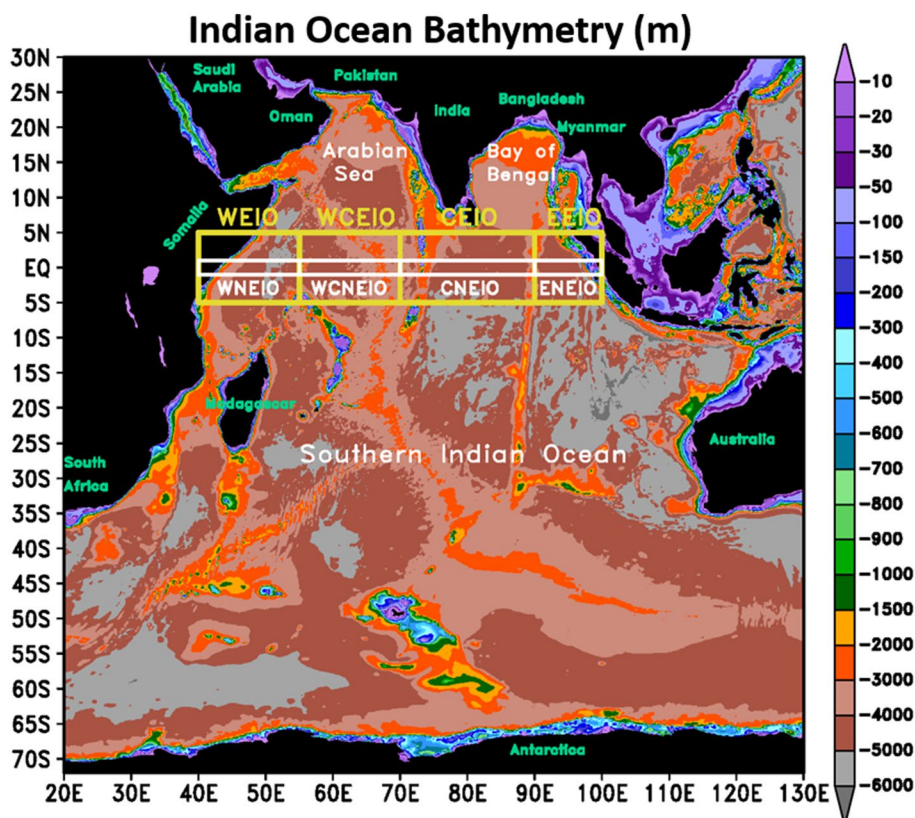
✉ C. Shaji
cshaji@coral.iitkgp.ac.in

¹ Centre for Oceans, Rivers, Atmosphere and Land Sciences (CORAL), Indian Institute of Technology, Kharagpur 721302, India

1 Introduction

The Indian subcontinent divides the northern Indian Ocean (IO) into two tropical oceans—the Arabian Sea (AS) in the west and the Bay of Bengal (BB) in the east. Both AS and BB communicate with the Equatorial Indian Ocean (EIO) at their southern boundary. The EIO, bounded by the latitudes 5°S and 5°N (Fig. 1), provides the source of energy for many unique atmospheric and oceanic processes and also for the coupling between the two. The EIO is entirely different from the equatorial Pacific and Atlantic oceans in

Fig. 1 Map of the Indian Ocean with different basins and bathymetry. The color shading indicates bathymetry (m), and data is based on Gridded Global Relief Data, the Earth Topography two arc-minute Version 2 (ETOPO2) v2 (National Geophysical Data Center, 2006). The boxes represent the various Equatorial Indian Ocean (EIO) regions considered for analysis



many respects. Unlike the other two major oceans where the equatorial winds are easterlies throughout the year, the semi-annually reversing monsoon winds dominate the EIO (Knox 1976; Senan et al. 2003) resulting in different surface and subsurface oceanic circulation characteristics (Schott et al. 2009; Rao et al. 2010). Usually, warm water coverage dominates the EIO with winds blowing eastward twice yearly during pre-monsoon and post-monsoon periods causing the convergence of warm water on the equator (Schott et al. 2002). In contrast, winds blowing over the equatorial Pacific and Atlantic Oceans are westward throughout the year, which generate Ekman divergence and occurrence of cold water on the equator.

The EIO surface winds play numerous cardinal roles in ocean dynamics and ocean–atmosphere coupling in the IO region. For example, the occurrence of periodic wind reversals in the EIO not only drives corresponding reversals in the upper ocean currents but also generates propagating signals such as Kelvin and Rossby waves that affect the upper ocean structure as remote effects (Potemra et al. 1991; Tsai et al. 1992; McCreary et al. 1993; Shankar et al. 2002; Shaji et al. 2003). The propagation of the Inter Tropical Convergence Zone (ITCZ) in the meridional direction reveals the seasonal variations of climatological EIO winds (Senan et al. 2003). During monsoon transition periods, ITCZ is mostly along the equator leading to the occurrence of high equatorial westerly winds. Remote driving through EIO winds

plays a significant role in monsoon rainfall over the Indian subcontinent (Yu et al. 1991; McCreary et al. 1993; Iskander et al. 2005; Francis and Gadgil 2009). The EIO winds are the significant forcing mechanism for driving the coastal currents such as the East India Coastal Current (EICC) in the BB and the West India Coastal Current (WICC) in the AS (Yu et al. 1991; McCreary et al. 1993, 1996). The EIO wind variability primarily causes the observed Sea Surface Height (SSH) anomalies near the eastern and northern coastal regions of the BB (Han and Webster 2002; Clark and Liu 1993). The zonal winds in the central EIO play a significant role in changing sea levels along the eastern EIO and thereby modulating the Lombok throughflow (Yamagata et al. 1996). Moreover, surface zonal winds averaged over the central EIO (60°E–90°E, 2.5°S–2.5°N) serve as an index for the Equatorial Indian Ocean Oscillation (EIOO) (Gadgil et al. 2004), wherein EIOO is considered as the atmospheric counterpart of the Indian Ocean Dipole (IOD) (Saji et al. 1999). Some studies have mentioned that the heating mechanism associated with the condensation of water vapor in deep convection cells (Webster 1972; Gill 1980) as well as the SST gradient (Lindzen and Nigam 1987) primarily governs the surface winds blowing over the tropical oceans. Thus, apart from the equatorial region, the effects of EIO winds are also experienced in the northern IO as a whole. Besides, there are also a few studies to understand the impact of the IO due to inter-annual variability of the EIO

winds. For instance, a study using ship observations during 1958–1997 has revealed the importance of pressure gradient force along the equator in maintaining the strength of the equatorial westerlies during monsoon transition periods (Hastenrath and Polzin 2004). Another study based on long-term observations (1948–1987) in the IO, including winds and surface currents, has revealed that the observed eastern African coastal rainfall anomalies are related to the Southern Oscillation during October–November through a combination of mechanisms that are mainly controlled by the equatorial westerlies (Hastenrath et al. 1993). The EIO winds in the eastern part within 80°E–90°E are essential for modulating Sea Surface Temperature Anomaly (SSTA) patterns along the Sumatra coast during El Niño–Southern Oscillation (ENSO) (Murtuggude and Busalacchi 1999). A study using long-term (1958–1998) seasonal anomalies of upper ocean heat content, SSTA, and surface wind stresses has identified an ocean–atmosphere coupled oscillation with a time scale of 2–5 years as the significant tropical IO climate variability signal (Huang and Kinter 2002). During this oscillation, equatorial zonal winds over the central and eastern regions, along with winds from the Southern Hemisphere, induce spatial SSTA and ocean heat content anomalies near the equator. During the mature phase of Positive Indian Ocean Dipole (PIOD) during September–October, easterly anomalies replace westerlies along the EIO (Vinayachandran et al. 2002). A recent study using both model and observations during 2001–2011 has shown that the inter-annual variability of zonal EIO wind stresses influence the inter-annual variability of eastern EIO upwelling (Chen et al. 2016). The easterly (westerly) wind stress anomalies along the equator tend to enhance (weaken) the eastern EIO upwelling.

The studies mentioned above have mostly focused on understanding the broad-scale features of the EIO winds. But, another important role of the EIO winds is to drive the Equatorial Undercurrent (EUC), which is a narrow, subsurface, swift-flowing eastward current, mostly occurring in the thermocline region and symmetrical about the equator with the surface current usually flowing in the opposite direction. Although EUC is a perennial current observed in the equatorial Pacific and Atlantic Oceans, it does not appear throughout the year in the EIO region. Both the local and remote forcing is responsible for the occurrence of EUC during February–April in the EIO. Easterlies in the EIO drive the westward flowing North Equatorial Current during NE monsoon period January–March, which results in accumulation of mass in the western EIO. Following this, EUC develops during February as a result of the establishment of eastward pressure gradient force in the thermocline region. But recent studies have identified that the EUC of the EIO is also influenced remotely by the equatorial waves, which arise due to the seasonally varying monsoonal, equatorial wind forcing

(Iskandar et al. 2009; Chen et al. 2015). Thus, a detailed study of the EUC in the IO necessitates good knowledge of the spatiotemporal variability of the EIO winds near to the equator. Such studies are not available in any of the previous attempts. This particular aspect prompted us to follow this research. The organization of the rest of this paper is as follows: Section 2 summarizes the data and methodology used. Section 3 provides the results and discussions, where first the annual cycle with seasonal variations and second the inter-annual variations of the EIO winds are dealt. We provide a summary and concluding remarks of the present study in Sect. 4.

2 Data and methodology

2.1 Data used

We have used the satellite-derived high-resolution ($0.25^\circ \times 0.25^\circ$) monthly CoastWatch winds provided by the National Oceanic and Atmospheric Administration (NOAA) (Freilich 2000; Lungu 2001). This dataset, covering the period from September 1999 to October 2009, is based on NASA's Quick Scatterometer (QuikSCAT) sensor. High resolution of this particular dataset helps to capture even small-scale wind variations, which are dynamically crucial to both the ocean and atmosphere but are not resolved in other observationally based wind atlases or reanalysis products such as NCEP–NCAR. We have prepared the monthly climatological winds using monthly data from the above period. In this study, we have used both monthly climatological winds as well as monthly winds from the above-noted multi-year period. The Dipole Mode Index (DMI) (<https://stateoftheocean.osmc.noaa.gov/sur/ind/dmi.php>) and Nino 3.4 index (<https://stateoftheocean.osmc.noaa.gov/sur/pac/nino34.php>) provide IOD and ENSO events occurred during September 1999–October 2009 and thereby understanding the behavior of the EIO winds during these unusual climatic events.

The Japanese 25-year Reanalysis (JRA-25) product (Onogi et al. 2007) provides monthly Sea Level Pressure data, with a horizontal resolution of $1.25^\circ \times 1.25^\circ$. Besides, for monthly SST, we have followed the ECMWF's Ocean Reanalysis System 4 (ORAS4) data, having a horizontal resolution of $1^\circ \times 1^\circ$ (Balmaseda et al. 2013). From the monthly time series of both these datasets, we have prepared monthly climatology of Sea Level Pressure and SST using individual monthly data of the two fields covering the period September 1999–October 2009.

2.2 Methodology

To obtain a quantitative estimate of wind direction variability, we have used a scalar meteorological field named the Wind Steadiness Factor (hereafter referred to as WSF) (Singer 1967). The WSF [expressed in percentage scale (%)] is defined as the ratio of Mean Resultant Wind Speed (MRWS) to Mean Scalar Wind Speed (MSWS). The expression for the same is given below:

$$\text{WSF (\%)} = \frac{\text{MRWS}}{\text{MSWS}} \times 100. \quad (1)$$

In Eq. (1), the numerator MRWS is the resultant wind speed of annual mean zonal wind component u and annual mean meridional wind component v :

$$\text{i.e. MRWS} = \sqrt{\left(\frac{1}{N} \sum_{i=1}^N u_i\right)^2 + \left(\frac{1}{N} \sum_{i=1}^N v_i\right)^2}. \quad (2)$$

The denominator MSWS in Eq. (1) represents the annual mean of scalar wind speed.

$$\text{i.e. MSWS} = \frac{1}{N} \sum_{i=1}^N \sqrt{u_i^2 + v_i^2}, \quad (3)$$

where u_i , v_i are the zonal and meridional components of the wind for the i th month, $N=12$, the total number of months (from January to December).

To understand the seasonal variability of winds near to the equator, we have performed Fast Fourier Transform (FFT) analyses (Jenkins and Watts 1968; Jakubasukas et al. 2001) on the zonal and meridional components of the EIO winds. For FFT analysis, the EIO winds are averaged in a latitudinal strip 1°S – 1°N , and the longitudinal stretch is taken from 45°E in the western to 100°E in the eastern EIO. Besides, to explain the dynamics of zonal winds near to the equator, we have also done FFT analyses separately on two other fields—momentum advection due to the cross-equatorial flow or interhemispheric circulation $\left(-v \frac{\partial u}{\partial y}\right)$ and zonal Sea Level Pressure gradient $\left(-\frac{\partial p}{\partial x}\right)$ —between 45°E and 100°E . Here, $\left(\frac{\partial u}{\partial y}\right)$ represents the meridional gradient of zonal wind and v is the cross-equatorial flow of wind.

On the inter-annual time scale, to understand how IOD and ENSO events affect the variabilities of the EIO winds, we have performed both correlation and Empirical Orthogonal Function (EOF) analyses. In the EIO, we have shown the correlations of (1) SSTA with DMI and Nino 3.4 index and (2) wind anomaly with DMI and Nino 3.4 index. The performance of EOF analysis on zonal winds during the period September 1999–October 2009 in the EIO helps to

determine the spatial patterns and temporal occurrences of the dominant modes of zonal wind variability in this region. Before computing EOF's, we have de-trended zonal wind anomalies, specifically to concentrate only on the significant wind variations occurring in the EIO. We have prepared the inter-annual monthly anomalies of zonal wind after subtracting the monthly climatology of zonal wind from the respective monthly zonal wind.

The EIO, as a whole, does not show a uniform spatial wind pattern in any particular season but instead exhibits sizeable spatial variabilities. Significant changes of winds, both in magnitude and direction, take place between the coastal regions and the central part of the EIO. Besides, different seasons mark its presence in various local areas of the EIO during different months. Therefore, by taking into account the regional and seasonal wind variations, we have divided the whole EIO into four local regions (Table 1 and Fig. 1) for studying the seasonal and inter-annual variabilities of the EIO winds. There are two boxes in both the coastal regions (west and east) and two in the central area (west-central and central). The arrangement of boxes like this manner in the EIO will facilitate to understand in greater detail the temporal and spatial wind variabilities occurring in each local region of the EIO.

3 Results and discussions

3.1 Annual mean and directional steadiness

Between 5°S and 5°N of the EIO, annual mean winds show the dominance of westerlies east of 60°E with strength increasing up to 90°E (Fig. 2a). High westerlies with magnitude up to 3 m s^{-1} cover in the central EIO from 80°E to 90°E . But east of 90°E , the intensity of annual mean winds decrease till the eastern limit of the EIO. West of 60°E , winds are southerlies or southeasterlies in the Southern Hemisphere and intense winds with maximum speed $> 3.5 \text{ m s}^{-1}$ occur near the Somalia region. Annual mean zonal wind pattern (Fig. 2b) reveals the dominance of westerlies east of 50°E , with well-marked maxima north of the equator within 80°E – 90°E where speed exceeds 3 m s^{-1} . Annual mean meridional wind pattern (Fig. 2c) exhibits mainly southerlies in the EIO, except a small region located north of the equator within 60°E – 80°E in the AS where meridional winds are weak northerlies with a maximum strength of up to 1.5 m s^{-1} . High southerlies persist west of 60°E , especially in the Somalia region where speed exceeds 2.5 m s^{-1} . The present analysis reveals that the distributions of southerlies and westerlies in the EIO primarily determine the annual mean wind pattern in this oceanic region. Thus, in the EIO, for any remarkable wind variations—seasonal, intra-seasonal, and inter-annual—, both the migrations and

Table 1 Different dynamically significant regions of the Equatorial Indian Ocean (EIO) with the respective areas.

| | | | | | |
|---|-------------------------------|--|---|--|--|
| Sl. No. | 1 | 2 | 3 | 4 | 5 |
| Name of the region | Equatorial Indian Ocean (EIO) | Western Equatorial Indian Ocean (WEIO) | Westcentral Equatorial Indian Ocean (WCEIO) | Central Equatorial Indian Ocean (CEIO) | Eastern Equatorial Indian Ocean (EEIO) |
| Area of the region | 40°E–100°E, 5°S–5°N | 40°E–55°E, 5°S–5°N | 55°E–70°E, 5°S–5°N | 70°E–90°E, 5°S–5°N | 90°E–100°E, 5°S–5°N |
| Sl. No. | 1 | 2 | 3 | 4 | 5 |
| Name of the near equator region | Near EIO (NEIO) | Western Near EIO (WNEIO) | Westcentral Near EIO (WCNEIO) | Central Near EIO (CNEIO) | Eastern Near EIO (ENEIO) |
| Area averaging of the near equator region | 1°S–1°N, 40°E–100°E | 1°S–1°N, 40°E–55°E | 1°S–1°N, 55°E–70°E | 1°S–1°N, 70°E–90°E | 1°S–1°N, 90°E–100°E |
| Sl. No. | 1 | 2 | 3 | 4 | 5 |
| Name of the zonally averaged region | Zonally Averaged EIO (ZAEIO) | Zonally Averaged Western EIO (ZAWEIO) | Zonally Averaged Westcentral EIO (ZAW-CEIO) | Zonally Averaged Central EIO (ZACEIO) | Zonally Averaged Eastern EIO (ZAEEO) |
| Zonally averaged longitudinal belt | 40°E–100°E | 40°E–55°E | 55°E–70°E | 70°E–90°E | 90°E–100°E |

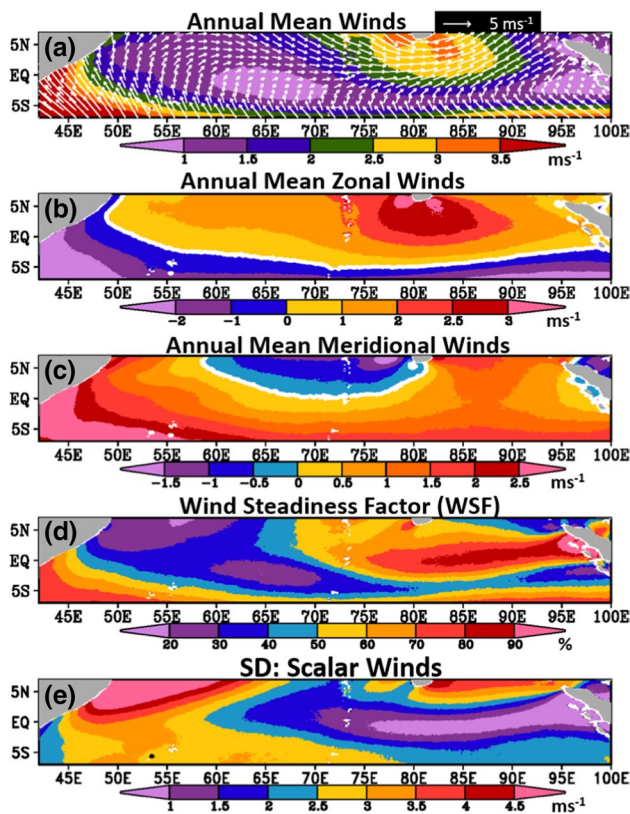


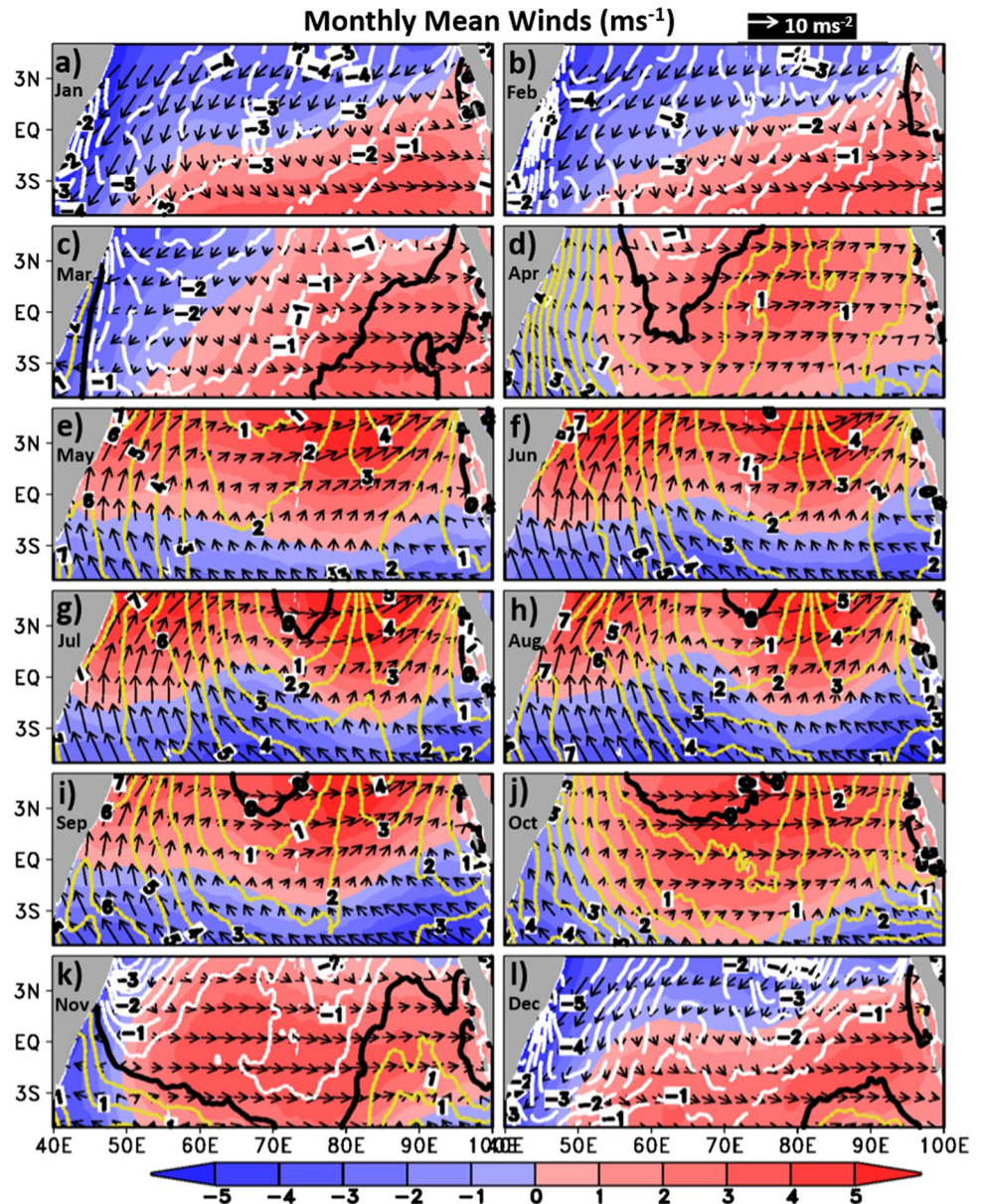
Fig. 2 Various wind fields in the Equatorial Indian Ocean (EIO) domain 5°S–5°N based on NOAA Coastwatch data. **a** Annual mean winds ($m s^{-1}$). The color shading indicates wind speed. **b, c** Annual mean zonal and meridional winds ($m s^{-1}$), respectively. **d** Wind steadiness factor, WSF (%). **e** The standard deviation of scalar winds ($m s^{-1}$)

the fluctuations of southerlies and westerlies play cardinal roles.

The westerlies bounded region east of 70°E in both hemispheres reveals high WSF with values between 50 and 90% (Fig. 2d). Coverage of high WSF in this region suggests that in the annual cycle either wind direction can be constant throughout the year or strong winds can blow in one direction during a specific period of the year and weak winds in the opposite direction during the rest of the year. It is evident that this region is occupied by high summer monsoon winds during initial 5 months from May to September in one direction and weak winter monsoon winds during latter 4 months from December to March in the opposite direction (Fig. 3). The eastern EIO in the Southern Hemisphere within 90°E–100°E exhibits triangular shaped low wind steadiness with WSF ranging from 30 to 40% (Fig. 2d), where winds reveal remarkable variations both in magnitude and direction from summer to winter monsoon (Fig. 3). The EIO west of 50°E shows the prevalence of small wind steadiness (WSF increases from 20 to 50% off Somalia region) in the Northern Hemisphere and high wind steadiness (WSF increases from 50 to 80% off Somalia region) in the Southern Hemisphere. This kind of WSF distribution west of 50°E of the EIO suggests that in this region winds are highly variable both in direction and magnitude in the Northern Hemisphere compared to the Southern Hemisphere winds.

The structure of standard deviations of wind speed exhibits high values north of the equator in comparison to the south of the equator (Fig. 2e). Maximum values remain in the western (west of 60°E) and east-central (between 80°E and 90°E) regions of the Northern Hemisphere. From this distribution, it is evident that in the EIO, seasonal variations

Fig. 3 a–l Monthly climatological winds (m s^{-1}) (vectors) over zonal (shaded), and meridional (contours) wind components (m s^{-1}) from January to December in the EIO. In the color shading, blue shaded negative values represent easterly winds, whereas red shaded positive values represent westerly winds. White contours indicate northerly winds, whereas yellow contours show southerly winds



of wind speed mostly confine to two prime areas located north of the equator—one in the western EIO at the west of 60°E and the other in the east-central longitudinal belt between 80°E and 90°E . However, small standard deviations prevail east of 80°E in the Southern Hemisphere near the equator, which indicates that seasonal wind speed variations are decidedly less in this part of the EIO.

3.2 Seasonal variations

The seasonal variations of the EIO winds occur during four periods: winter or NE monsoon (December–March), summer or SW monsoon (June–September), and transitions between the two monsoons—pre-monsoon or spring (April–May) and post-monsoon or fall (October–November).

Figure 3 illustrates the monthly climatological winds with zonal (shaded) and meridional (contour) components. During December–March, north of the equator, NE monsoon winds blow with moderate strength, which then turns to northwesterlies after crossing the equator. However, during March–April, winds calm down in the EIO region. The noted feature during April is the presence of westerlies east of 55°E with core near the equator and decreasing strength away from the equator. At this time, the maximum westerlies prevail in the central EIO within 70°E – 90°E . In May, westerlies are very intense and occupy a more extensive area north of the equator. Also, in the EIO, winds gradually switch from NE to SW monsoon condition in May. During SW monsoon period June–September winds completely reverse in the EIO. At this time, north of the equator, summer

monsoon winds blow steadily from the southwest. In the EIO, summer monsoon winds are much stronger than winter monsoon winds. For example, in the western EIO, summer (winter) monsoon winds at the peak of the season during July–August (January–February) attain speed $> 9 \text{ m s}^{-1}$ ($\sim 7 \text{ m s}^{-1}$) and cover a more extensive (smaller) western area. During SW monsoon, southeast trades are active in the western part and become southwesterlies after crossing the equator with maximum speed $> 9 \text{ m s}^{-1}$. These winds are the highest of the three oceans during the summer. After the withdrawal of SW monsoon, winds again calm down in the EIO during fall transition period October–November. The westerlies blow east of 55°E at the equator during spring (April–May) and fall (October–November) transition periods with maximum winds in the central EIO within 60°E – 90°E . During spring (fall), strong westerlies occur in May (October). Also, westerlies in the EIO are well developed and stronger during fall (maximum speed of 5 m s^{-1}) compared to spring (maximum speed of 4 m s^{-1}).

The monthly climatological meridional winds (contours in Fig. 3) reveal specific striking characteristics. During the winter monsoon, northerlies first appear in October north of the equator in the AS (Fig. 3j) except its western part. As winter advances, northerlies (white contours) gradually spread more toward the south. During December–February, northerlies cover the entire EIO and strengthen in January with the maximum northerly component $> 5 \text{ m s}^{-1}$ in the Somalia region. However, in April, southerlies (yellow contours) replace northerlies almost everywhere in the equatorial region (Fig. 3d), except in the central AS. In May, southerlies occupy the whole EIO and further intensify during SW monsoon period June–August (Fig. 3f–h), with a maximum of 7 m s^{-1} during July–August in the Somalia region. The strength of SW monsoon southerlies starts diminishing in September. Throughout the year, meridional winds are weak in the eastern EIO compared to the western EIO. During peak NE monsoon (January–February) and SW monsoon (June–August) periods, meridional winds exhibit a zonal gradient from west to east in the EIO.

In the EIO, meridional winds exhibit cross-equatorial flow due to the movement of the ITCZ north and south of the equator. For the variability of winds in the EIO, meridional winds play a significant role only in the western and eastern boundaries of the EIO. For example, in the western boundary, the presence of the African highlands plays an integral role in modulating the speed and structure of the cross-equatorial flow. East African highlands, Madagascar mountains, land–sea contrast, and the beta effect altogether play essential roles in determining the strength of the cross-equatorial winds in the western EIO (Krishnamurti et al. 1976). Due to the presence of African highlands, during SW monsoon, the strong cross-equatorial southeasterlies and southerlies remain only in the western EIO between 40°E

and 60°E (Chakraborty et al. 2009). Besides, in the western EIO, the African highlands also block the strong zonal winds emanating from the African continent, thereby enhancing the meridional winds in the western boundary.

The monthly climatological zonal winds (shading in Fig. 3) indicate that during October–November, well-organized westerlies occur in the majority of the EIO located east of 55°E with strong westerlies in the central region between 60°E and 90°E (Fig. 3j, k). However, at this time, easterlies occupy the area west of 55°E . With the progress of winter monsoon from November onward, easterlies spread more toward east and north and strengthen further in the western EIO. By January–February, the EIO north of the equator shows the coverage of winter easterlies (Fig. 3a, b), with intense winds seen west 80°E . During April–May, westerlies replace easterlies in the majority of the EIO region (Fig. 3d, e). In May, westerlies cover the entire northern EIO and southern latitudes near to the equator. During the summer monsoon, zonal winds are westerlies north of the equator (Fig. 3f–i). In July, westerlies reach their peak with a maximum speed of about 6 m s^{-1} , and in September become weak. Also, zonal winds show that during the height of SW monsoon in June–August, there are two westerly maxima regions located in the western and east-central EIO (Fig. 3f–h). In both areas, the maximum magnitude reaches about 6 m s^{-1} . During September, westerlies in the western EIO weaken. However, in the east-central EIO, westerlies further strengthen and broaden in September, with the presence of strong westerlies during October–November. The westerlies are active at and near the equator east of 55°E during monsoon transition periods April–May and October–November, with the maximum winds in the central EIO within 60°E – 90°E . During the spring transition period, westerlies are stronger in May; while during the fall transition period, stronger westerlies occur in October. But on average, in the EIO, strong westerlies arise during fall compared to spring.

Seasonal variability of the EIO winds demonstrates that the signatures of the four cardinal seasons occur during different periods in various local regions. Thus, based on the seasonal wind variability, four longitudinal belts are identified in the EIO—WEIO, WCEIO, CEIO, and EEIO—(Fig. 1 and Table 1). In these local regions, the four cardinal seasons occur during different periods (Table 2). Although seasonal wind variations in the WEIO and WCEIO are much similar, magnitude-wise the WCEIO winds are weaker compared to the WEIO winds. But in the CEIO, winds are weak nearer the equator (especially within 1°S – 1°N) during SW and NE monsoons, while high winds occur in this region during monsoon transition periods.

For further analysis of meridional winds, we have selected area-averaged boxes only near the boundaries of the EIO because meridional winds are weak in the

Table 2 Seasonal appearance of winds at different regions of the Equatorial Indian Ocean (EIO)

| Seasons | WEIO | WCEIO | CEIO | EEIO |
|--------------|----------------|------------------|-------------------|-------------------|
| NE monsoon | December–March | December–March | December–February | January–February |
| Pre-monsoon | April | April | March–April | March–April |
| SW monsoon | May–October | May–September | May–September | May–October |
| Post-monsoon | November | October–November | October–November | November–December |

central region. But for zonal winds, we have chosen four area-averaged boxes covering the boundaries and central parts of the EIO. Figure 4a shows annual cycles of area-averaged meridional winds at various EIO regions, namely NEIO, WNEIO, WCNEIO, CNEIO, and ENEIO (Table 1). Though oscillations of meridional winds are the same in all the above-selected domains, their amplitudes are entirely different. The annual cycles of meridional winds at NEIO and WCNEIO regions are much similar even amplitude-wise also. During December–March, all areas exhibit weak northerlies, which then gradually switch over to southerlies from April onward with its strengthening during the SW monsoon period and persistence till October. The WNEIO shows strong southerlies with a maximum strength of about 7.5 m s^{-1} in June. However, ENEIO domain shows weak meridional winds throughout the year. To understand further the latitudinal evolution of meridional winds between the western and eastern EIO regions, time latitude plots of zonally averaged demeaned seasonal cycles of meridional winds are presented (Fig. 4b–e) in four selected domains—ZAEIO, ZAWEIO, ZAWCEIO, and ZAEIO—(Table 1). To obtain demeaned seasonal cycle, we have subtracted the annual mean of meridional wind from the monthly climatological meridional wind. The resultant meridional wind shows monthly variations about the annual mean, with positive (negative) anomalous wind implying anomalous southerly (northerly) wind. The switchover between anomalous southerlies and anomalous northerlies co-occurs throughout the latitudinal stretch 5°S – 5°N in the ZAEIO (Fig. 4b). The anomaly patterns of meridional winds are similar in the ZAWEIO (Fig. 4c) and ZAWCEIO (Fig. 4d) areas, but not in ZAEIO (Fig. 4e). The domains ZAEIO, ZAWEIO, and ZAWCEIO reveal the presence of northerly wind anomalies during November–April in all latitudes, with peak values during January–February. By mid-April, southerlies replace northerlies in these domains. Meridional wind anomalies are stronger in the ZAWEIO region, with higher magnitudes during both NE and SW monsoons. In the ZAEIO domain, northerlies first appear at the northern latitudes during November and then extend toward southern latitudes. By December, northerlies occupy the whole latitudinal strip of the ZAEIO domain. Reversal of northerlies in the ZAEIO region first occurs in the Northern Hemisphere during mid-March and then gradually proceeds toward the south with the march of the season.

Figure 4f shows the annual cycles of area-averaged zonal winds in the selected five near EIO regions. Among the five regions, four are the same as the ones used earlier for the analysis of meridional winds—i.e., NEIO, WNEIO, WCNEIO, and ENEIO. The additional fifth region considered is the central near EIO (CNEIO) (Table 1). Concerning the area-averaged zonal wind, the annual cycles in the NEIO and CNEIO areas show excellent correspondence. However, WNEIO, WCNEIO, and ENEIO regions demonstrate different annual cycles. In the NEIO and CNEIO regions, peak westerly winds occur during monsoon transition months May and October. In the eastern part ENEIO, zonal winds are weak, and the annual cycle is also entirely different. Most of the year, ENEIO shows the predominance of westerlies, except for the occurrence of weak easterlies during July–August. But the western part WNEIO shows strong westerlies during SW monsoon and strong easterlies during NE monsoon.

It turns out that the zonal wind component is the significant contributor to the total wind field in most of the EIO regions, except the western and eastern limits. Therefore, to understand the evolution of zonal wind at various local areas in the EIO, the time latitude diagrams of the seasonal cycles of demeaned zonal wind are presented (Fig. 4g–k) in five zonally averaged domains (Table 1). In these five domains, four are same as the ones mentioned earlier—i.e., ZAEIO (Fig. 4g), ZAWEIO (Fig. 4h), ZAWCEIO (Fig. 4i), and ZAEIO (Fig. 4k). The additional fifth domain selected is the zonally averaged central EIO domain (ZACEIO) (Fig. 4j). During winter, ZAEIO shows the appearance of anomalous easterly winds first in the Northern Hemisphere in December, and then with the progress of the season, anomalous easterlies gradually extend southward up to 2°S (Fig. 4g). But in other local regions, the latitudinal evolutions of zonal winds are not alike. For instance, the western domain ZAWEIO shows first the arrival of anomalous easterly winds during October north of 2°N , and with the progress of winter monsoon, easterlies extend more toward the equator with enhanced intensity (Fig. 4h). The winter anomalous easterly winds first appear in the western EIO region (Fig. 4h) and then proceed toward the eastern EIO region (Fig. 4k). During January–February, the strongest anomalous easterly winds blow over the north of 2°S in the western (Fig. 4h), west-central (Fig. 4i), and central (Fig. 4j) EIO regions with maximum easterly wind anomaly

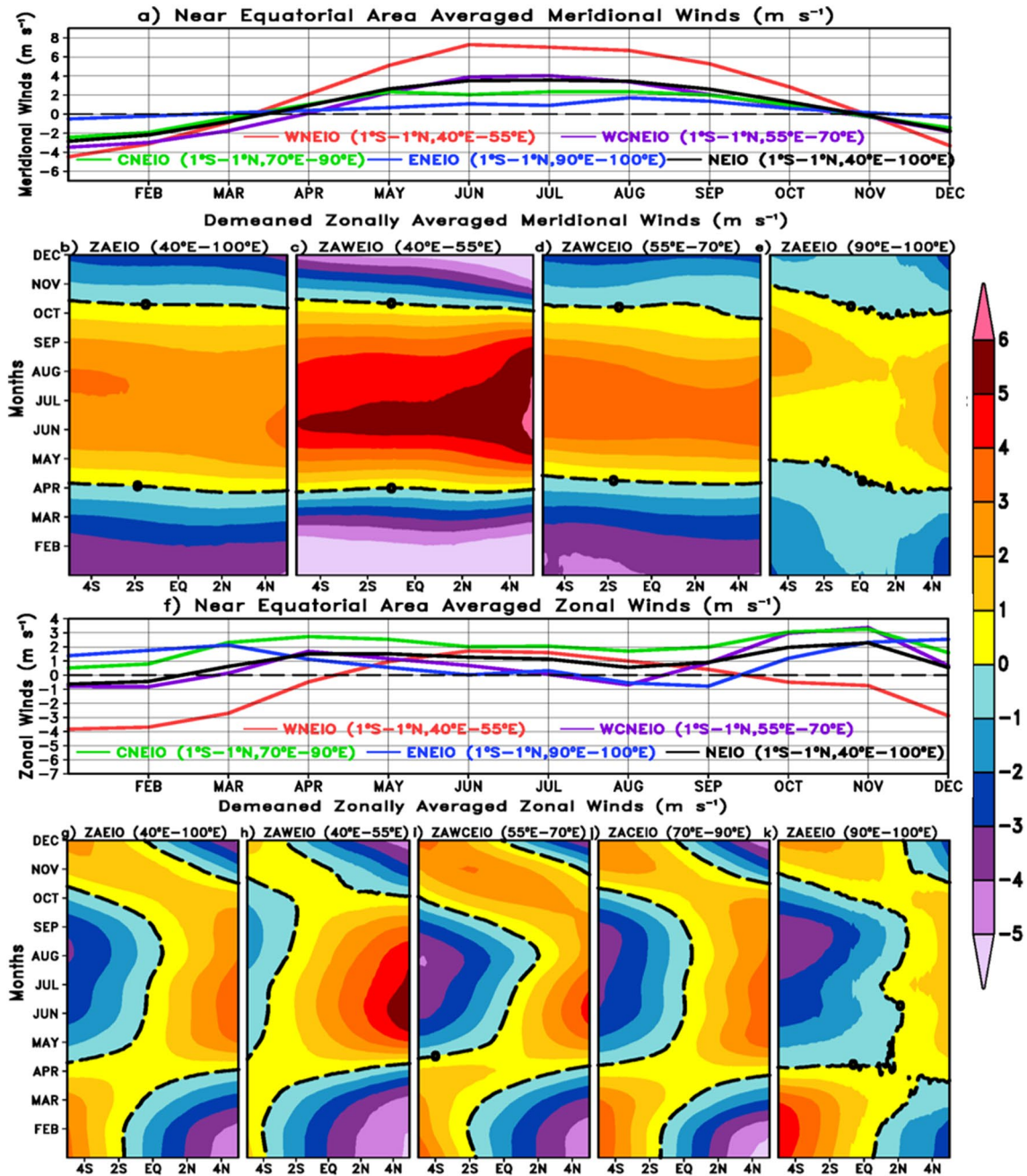
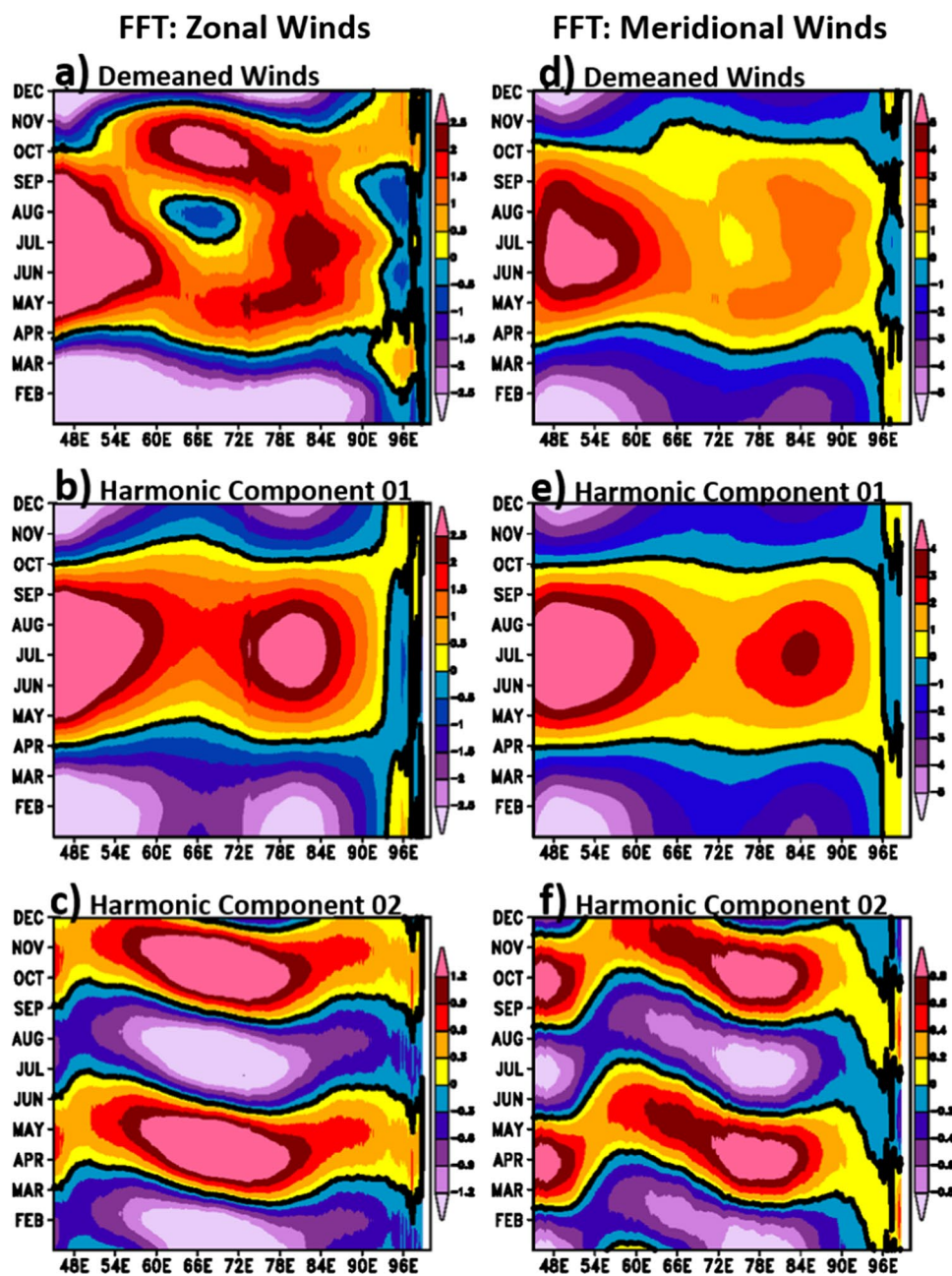


Fig. 4 a–e The upper two panels show the **a** Annual cycles of near EIO area averaged meridional wind ($m s^{-1}$) for five selected regions—western near EIO (WNEIO) (area averaged at $1^{\circ}S-1^{\circ}N$, and $40^{\circ}E-55^{\circ}E$) (solid red curve), west-central near EIO (WCNEIO) (area averaged at $1^{\circ}S-1^{\circ}N$, and $55^{\circ}E-70^{\circ}E$) (solid purple curve), central near EIO (CNEIO) (area averaged at $1^{\circ}S-1^{\circ}N$, and $70^{\circ}E-90^{\circ}E$) (solid green curve), eastern near EIO (ENEIO) (area averaged at $1^{\circ}S-1^{\circ}N$, and $90^{\circ}E-100^{\circ}E$) (solid blue curve), and whole near EIO (NEIO) (area averaged at $1^{\circ}S-1^{\circ}N$, and $40^{\circ}E-100^{\circ}E$) (solid black curve)—. **b–e** The latitude Vs month representations of monthly demeaned (by removing climatological annual mean from monthly climatology) meridional wind ($m s^{-1}$) for four zonally averaged domains of the EIO. Monthly evolutions of demeaned

meridional winds at various latitudes can be identified in the four domains. **b** Zonally averaged EIO domain (ZAEIO) (averaged within $40^{\circ}E-100^{\circ}E$). **c** Zonally averaged western EIO domain (ZAWCEO) (averaged within $40^{\circ}E-55^{\circ}E$). **d** Zonally averaged west-central EIO domain (ZAWCEIO) (averaged within $55^{\circ}E-70^{\circ}E$). **e** Zonally averaged eastern EIO domain (ZAEIO) (averaged within $90^{\circ}E-100^{\circ}E$). In the lower two panels **f** represents the annual cycles of near EIO area averaged zonal winds ($m s^{-1}$) for the five selected regions, and **g–k** represent the latitude Vs month representations of monthly demeaned zonal wind ($m s^{-1}$) for five zonally averaged domains of the EIO. The fifth domain of the bottom panel **j** represents the zonally averaged central EIO domain (ZACEIO) (zonally averaged between $70^{\circ}E$ and $90^{\circ}E$)

Fig. 5 **a, d** The longitude Vs month plots of the demeaned monthly zonal and meridional winds (m s^{-1}) respectively. **b, c, e, f** The first or fundamental harmonic (annual harmonic), and the second harmonic (semi-annual harmonic) respectively of the Fast Fourier Transform (FFT) analysis of **b, c** zonal and **e, f** meridional winds (m s^{-1}). The data is averaged between latitudes 1°S and 1°N and covering longitudes 45°E – 100°E in the EIO



reaching $> 5 \text{ m s}^{-1}$. In the western area ZAWEIO, anomalous easterlies during winter are the strongest and show maximum southward extension (Fig. 4h). But the eastern part ZAEIO shows feeble easterly anomalies during winter with a maximum of about 3 m s^{-1} north of the equator (Fig. 4k). By April, anomalous westerlies appear north of the equator in all selected local regions. The westerly anomalies further intensify during May–August, with high anomalies in the ZAWEIO, ZAWCEIO, and ZACEIO regions (with a maximum westerly anomaly of 5 m s^{-1}) and weak anomalies in the eastern ZAEIO region (with a maximum westerly anomaly of 2 m s^{-1}). This result reveals that the spatial

patterns of zonal wind anomaly are almost identical in the whole EIO region ZAEIO (Fig. 4g) and in the central EIO region ZACEIO (Fig. 4j). Therefore, the zonal wind variabilities occurring in the central area ZACEIO remain as a decisive factor to understand the zonal wind variations taking place in the whole EIO region ZAEIO.

3.2.1 Fast Fourier Transform (FFT) analysis

The equatorial monthly climatological zonal and meridional winds are dominated by the contributions from the time-averaged mean and dominant harmonic components,

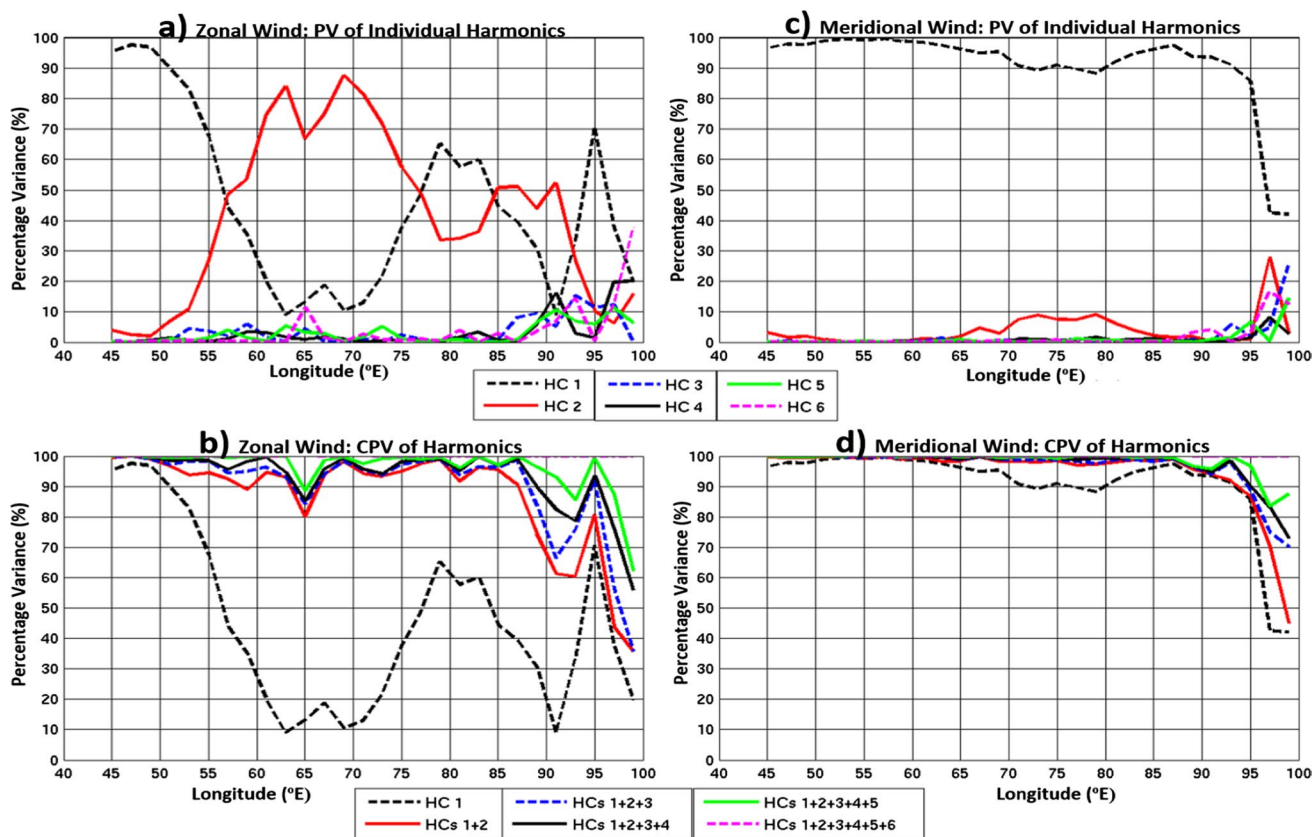


Fig. 6 a, c The percentage of variance explained by the individual harmonic components of zonal and meridional winds respectively at various longitudes in the EIO from the FFT analysis. b, d The cumulative percentage of variance of harmonic components of zonal and

meridional winds respectively, which are essentially sum of percentage of variance of individual harmonics. Altogether, six individual harmonic components (a, c) and their cumulative effects (b, d) are plotted

of which the most significant are annual (Fig. 5b, e) and semi-annual (Fig. 5c, f).

3.2.1.1 Zonal winds Figure 5a provides the temporal evolution of monthly anomaly (obtained after subtracting the annual mean from monthly data) of zonal winds averaged between 1°S and 1°N in the EIO region. The first harmonic component is the annual harmonic (Fig. 5b). It is evident that the spatial patterns are akin in both the distributions (Fig. 5a, b) and reveal the following signatures: West of 55°E, easterlies occur during November–March and westerlies during April–September. In the western EIO, westerlies are at their peak during the peak of SW monsoon in July–August, whereas easterlies in this region strengthen during the height of NE monsoon in January–February. The annual component of zonal winds (Fig. 5b) exhibits a maximum amplitude near the western boundary of the EIO. This feature can be attributed to the reversing monsoon winds off Somalia region. Besides, there are also two relatively smaller zonal wind maxima regions with core values located at 80°E in the central and at 96°E in the eastern boundary of the EIO. The peak zonal winds in these two local regions

occur due to monsoon winds extending southward from south of Sri Lanka and along the Indonesian coast, respectively. The semi-annual harmonic of zonal winds, however, exhibits a simple structure with a single maximum located in the mid-ocean (Fig. 5c). The central EIO within 60°E–80°E shows the highest amplitude of the semi-annual variations of zonal winds. In this longitudinal belt, strong easterlies occur during peak winter (January–February) and summer (July–August) monsoons, whereas strong westerlies during monsoon transition periods in spring (April–May) and fall (October–November).

For zonal winds, the contributions from the individual harmonics (Fig. 6a) and the cumulative percentage variances of harmonics (Fig. 6b) reveal the following characteristics: West of 55°E, the annual harmonic is significant (>70%) and reaches a maximum of about 98% at 48°E (Fig. 6a). But the semi-annual harmonic component in the same region is weak (<30%). In the western basin, it is furthermore evident that the total variations of zonal winds occur due to the combined effect of significant contribution from the annual harmonic and minor contribution from the semi-annual harmonic. However, the contributions from higher

harmonics 3–6 are too insignificant to be considered in this region. In the central basin from 60°E to 75°E, the semi-annual harmonic component is above 60% and attains two maxima at 63°E and 69°E with 85% and 88% contributions, respectively (Fig. 6a). It is noteworthy that in the central EIO basin also the contributions from the semi-annual and annual harmonics—significant from semi-annual and minor from annual—are enough to explain the total zonal wind variations. Like western EIO, in the central basin also higher harmonics are too weak to contribute effectively. From 75°E to 90°E, the annual and semi-annual harmonics provide more or less equally. Beyond 90°E in the eastern EIO, the annual harmonic is again significant. Altogether, the annual and semi-annual harmonics are good enough to illustrate the total variations in the annual cycle of zonal winds throughout the EIO (Fig. 6a, b). Higher frequency harmonics, however, do not have an organized structure. Their contributions for the total zonal winds are insignificant and thus can be avoided. Particularly in the eastern boundary of the EIO, higher frequency harmonics appear to be noise (Fig. 6a, b).

3.2.1.2 Meridional winds Similar spatial patterns exist in the temporal evolution of the anomalies (Fig. 5d) and the annual harmonic (Fig. 5e) of the EIO meridional winds. Both the distributions (Fig. 5d, e) show that throughout the EIO, annual variations are apparent in the meridional winds with the maximum amplitude confined to the west 60°E, and decreasing in strength from 60°E to 72°E. Also, there is a relatively secondary peak with its core near 85°E. Distribution of the annual harmonic of meridional winds reveals the prevalence of northerlies during November–March and southerlies during May–September. Moreover, for the annual harmonic, the switchover from northerlies to southerlies occurs almost simultaneously throughout the EIO. From the annual harmonic distribution, it is also apparent that amplitudes of meridional winds are quite higher than the amplitudes of zonal winds. The second harmonic of meridional winds, like zonal winds, reveals semi-annual variations with its clear signatures in the western EIO west of 54°E, eastern EIO east of 95°E, and in the central region between 60°E and 90°E (Fig. 5f). Since there is an upslope from 90°E to 60°E concerning the occurrence of the semi-annual harmonic of meridional winds, it is evident that the switchover between southerlies and northerlies does not co-occur everywhere in the central part of the EIO.

Individual harmonics of meridional winds indicate that west of 90°E, the annual harmonic is the predominant one with percentage variance above 80% (Fig. 6c). The annual harmonic reaches upper limit west of 65°E and near 87°E. But the semi-annual harmonic, though very insignificant, provides minor contributions at the east of 95°E (below 28%) and in the central ocean between 65°E and 85°E (below 10%). Overall, the annual harmonic component can

explain how the annual cycle of meridional winds varies in the EIO region (Fig. 6c, d). Like zonal winds, east of 95°E of the EIO, higher frequency components seem to be noise and thus can be avoided.

3.2.1.3 Zonal sea level pressure gradient and momentum advection An earlier study has noted the significance of momentum advection arising due to the cross-equatorial flow ($-v\frac{\partial u}{\partial y}$) as a result of the meridional displacement of the ITCZ for governing the seasonal cycles of zonal wind over the equatorial Atlantic Ocean (Okumura and Xie 2004). Henceforth, we refer the term ($-v\frac{\partial u}{\partial y}$) as the momentum advection. Besides, the zonal Sea Level Pressure gradient term ($-\frac{\partial p}{\partial x}$) also plays an integral role in maintaining winds over the EIO. Therefore, to understand the functions of these two terms for the maintenance of the EIO winds, we have performed the FFT analyses on these two fields. Figure 7 illustrates the monthly evolutions of the annual and semi-annual harmonics of the momentum advection (Fig. 7a, d) and the zonal Sea Level Pressure gradient (Fig. 7b, e). The bottom subplots in Fig. 7 illustrate the combined effects of the two fields in the annual (Fig. 7c) and semi-annual harmonics (Fig. 7f). The annual and semi-annual harmonics of both the above fields—momentum advection and zonal Sea Level Pressure gradient—indicate significant variations west of 60°E (Fig. 7). During November–March, in the western EIO between 40°E and 60°E near the equator (1°S–1°N), the annual harmonic of momentum advection shows westerly acceleration (Fig. 7a) while that of zonal Sea Level Pressure gradient displays easterly acceleration (Fig. 7b). During the rest of the period also, in the same longitudinal belt, the annual harmonic of both the fields show opposite accelerations. However, the pattern of the resultant acceleration of the annual harmonic (Fig. 7c) mainly resembles the zonal Sea Level Pressure gradient pattern (Fig. 7b). One can also notice that eastward of 60°E near the equator (1°S–1°N), the annual harmonics of the two fields (Fig. 7a, b) and their resultant (Fig. 7c) do not show any significant accelerations.

During the peak periods of NE monsoon (December–February) and SW monsoon (June–August) seasons, between 45°E and 60°E of the western EIO, the semi-annual component shows the occurrence of an easterly acceleration of the momentum advection (Fig. 7d) and westerly acceleration of the zonal Sea Level Pressure gradient (Fig. 7e). However, in the same longitudinal belt, during the transition periods April–May and October–November, the semi-annual harmonic of the momentum advection shows westerly acceleration (Fig. 7d), in contrast to the easterly acceleration of the zonal Sea Level Pressure gradient (Fig. 7e). During the four seasons, west of 60°E, the pattern of the resultant acceleration of the semi-annual harmonic (Fig. 7f) resembles

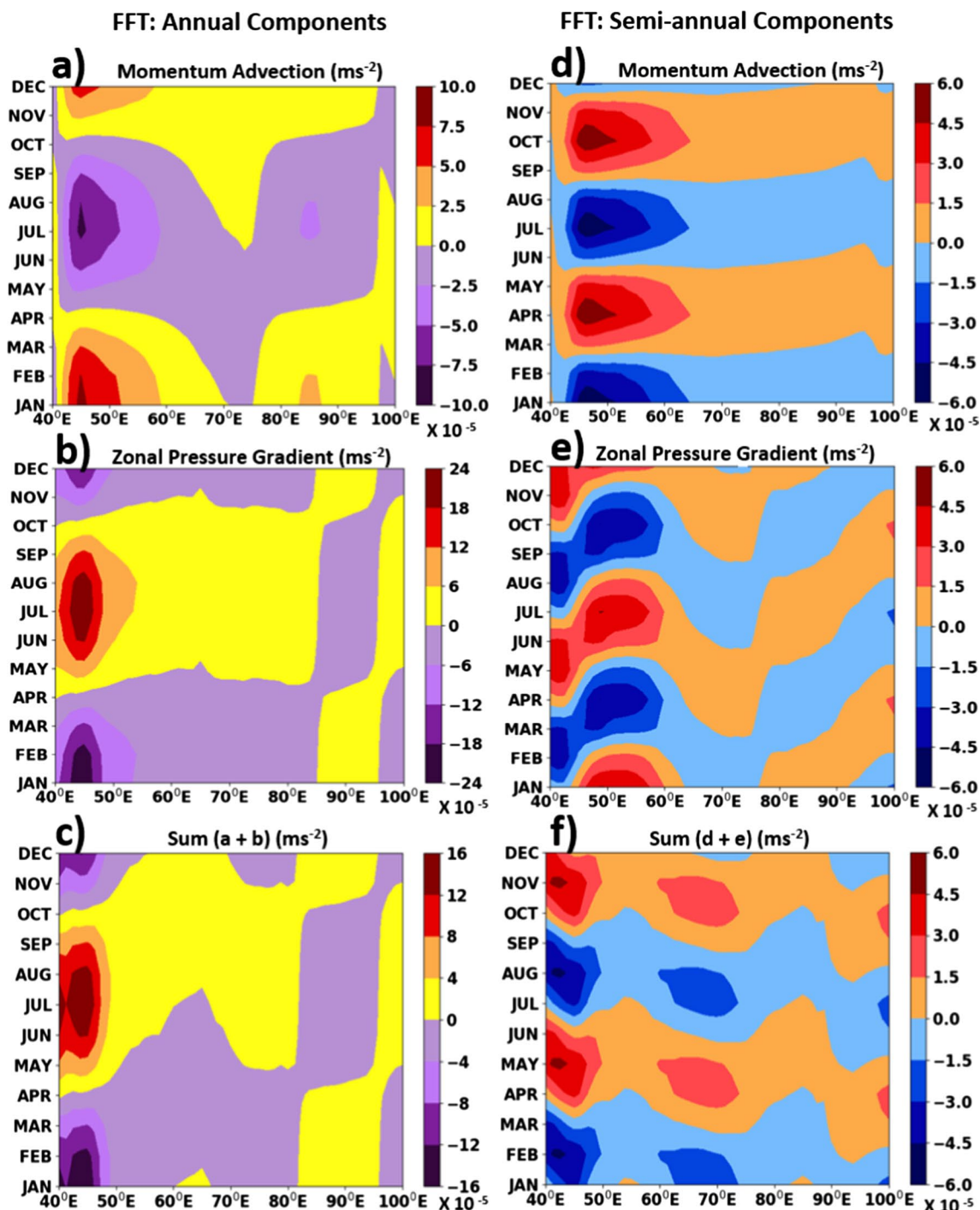


Fig. 7 The longitude Vs month plots of the first or annual harmonic of the FFT analysis of **a** momentum advection of zonal winds $-v \frac{\partial u}{\partial y}$ ($m s^{-2}$) and **b** zonal sea level pressure gradient $-\frac{\partial p}{\partial x}$ ($m s^{-2}$). The longitude Vs month plots of the second or semi-annual harmonic of the FFT analysis of **d** momentum advection of zonal winds and **e** zonal

Sea Level Pressure gradient. The bottom subplots represent the sum of the above two fields for the **c** annual (sum of **a**, **b**) and **f** semi-annual (sum of **d**, **e**) harmonics of the FFT analysis. All plots are made in the near EIO area by averaging between latitudes $1^{\circ}S$ and $1^{\circ}N$

the momentum advection pattern (Fig. 7d). The strength of the meridional winds governs the momentum advection in the western EIO, especially off the East Africa coast. The

semi-annual harmonic of the momentum advection (Fig. 7d) shows strong easterly acceleration during June–August west of $60^{\circ}E$, which is associated with the strong Somali Jet

(Findlater 1969) off the East Africa coast during this period (Fig. 3). Also, during January–February, meridional winds are stronger in the western EIO compared to the central EIO, which results in a stronger easterly acceleration in the western EIO. West of 60°E of the EIO, SST anomalies also play a significant role in the build-up of the zonal Sea Level Pressure gradient. In the western EIO, the climatological SST anomalies are cold during winter and summer seasons and warm during monsoon transition periods (Murtugude and Busalacchi 1999). The occurrence of strong cooling during winter and summer in the west of 60°E results in high Sea Level Pressure in the western EIO, which establishes westerly acceleration of the zonal Sea Level Pressure gradient. However, during transition periods, the warm SST anomalies in the western EIO results in low Sea Level Pressure in that region and thereby easterly acceleration of the zonal Sea Level Pressure gradient.

The FFT analysis presented in this section reveals that both annual and semi-annual harmonics of momentum advection and zonal Sea Level Pressure gradient are active in the western EIO west of 60°E throughout the year. For the annual harmonic, especially west of 50°E, both the accelerations show opposite directions. The resultant acceleration of the annual harmonic (Fig. 7c) mainly resembles that of the zonal Sea Level Pressure gradient (Fig. 7b), indicating the predominance of this term. West of 50°E, throughout the year, the semi-annual harmonics of both momentum advection and zonal Sea Level Pressure gradient are in opposite directions, and the resultant resembles that of momentum advection. In the central EIO between 60°E and 80°E, the semi-annual components of both the fields are weak but show similar kind of accelerations. As a result of these peculiar distributions of the two acceleration terms in the EIO, the zonal winds are weak in the western EIO west of 60°E, but they are stronger in the central EIO between 60°E and 80°E.

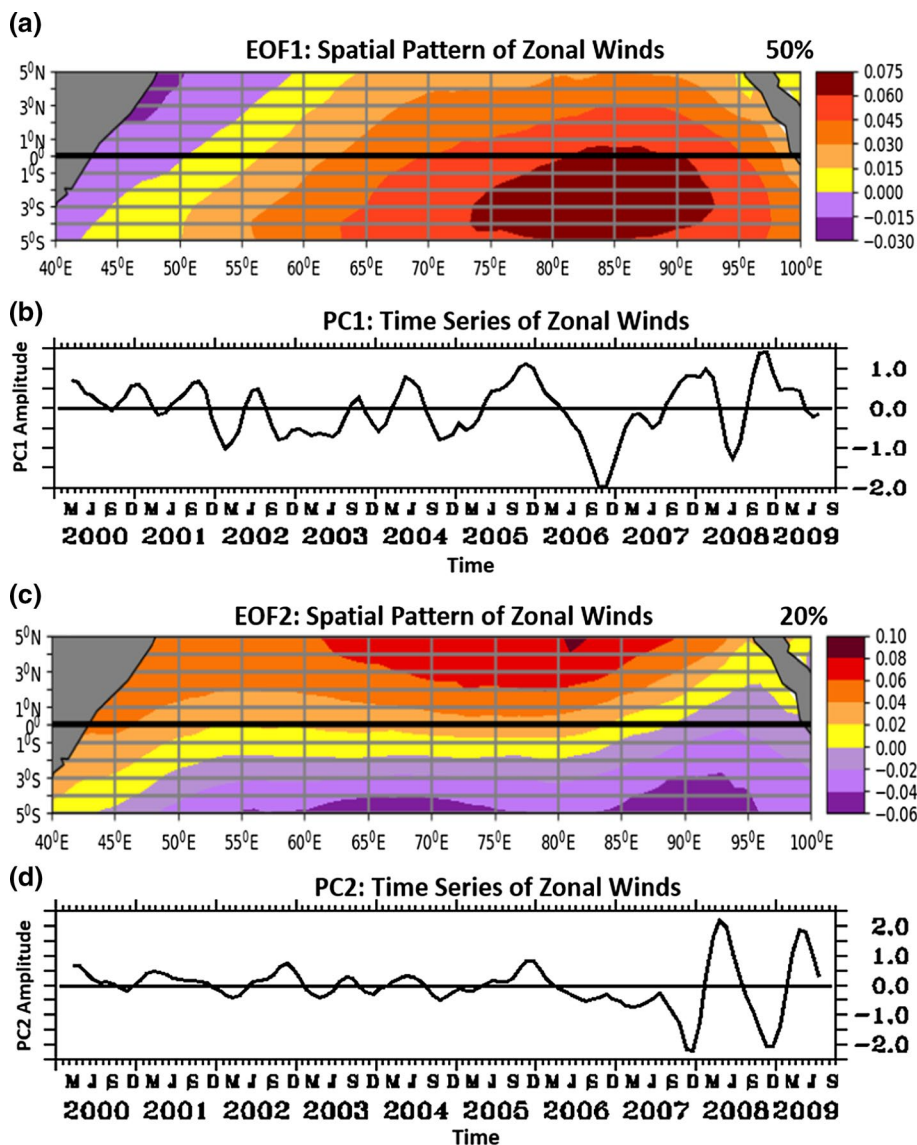
3.3 Inter-annual variations

The predominant inter-annual variations occurring in the EIO are associated with ENSO and IOD climate modes (Schott et al. 2009). We have used NOAA Coast Watch data during September 1999–October 2009 to study the inter-annual variability of surface winds over the EIO. To understand the general features of the inter-annual variability and the impacts of IOD and ENSO on the EIO zonal winds, we have performed the EOF analysis of this component in the EIO region during September 1999–October 2009 (Fig. 8). The spatial pattern associated with the first EOF mode (EOF1) of zonal winds captures around 50% of the total variance of zonal winds (Fig. 8a). The EOF1 shows positive loading almost in the entire EIO region, except near the extreme western boundary, with maxima in the east-central

part between 80°E and 90°E south of the equator. Notably, this mode resembles the spatial pattern of zonal winds usually taking place over the EIO during the monsoon transition periods of spring and fall. The spatial pattern of the second EOF mode (EOF2) of zonal winds, however, explains about 20% of the total variance of zonal winds (Fig. 8c). The spatial pattern of EOF2 exhibits a meridional gradient, with a weaker magnitude in the central ocean between 55°E and 80°E near the equator in the Southern Hemisphere, and getting stronger away from the equator in both the hemispheres. Moreover, EOF2 mostly represents the inter-annual variability of zonal winds occurring during the summer season in the EIO since the spatial distribution of this mode resembles the usual zonal wind pattern observed during summer. The time series of the first PC (PC1) (Fig. 8b) reveals anomalously strong negative values in some years, especially at the end of the year 2006, which was a PIOD year. Based on both the spatial pattern of EOF1 (Fig. 8a) and its corresponding PC1 (Fig. 8b), it is apparent that easterly wind anomalies occur during the PIOD year 2006 in almost the entire EIO, with the presence of the most substantial magnitude between 75°E and 92°E in the east-central region. The time series of the second PC (PC2) (Fig. 8d) does not show any significant variation during IOD years like 2006 but shows changes during 2007–2008, a period when both PIOD and La-Niña events co-occurred. Therefore, the present analysis demonstrates that the EOF2 of zonal winds does not highlight the IOD events, but instead shows variations during the combined PIOD and La-Niña episodes.

To further understand the impacts of IOD and ENSO on the wind variability in the EIO, we have also carried out separate correlation analyses of SSTA and wind anomalies with the DMI and Nino 3.4 index (Fig. 9). Figure 9a shows DMI (red curve) and Nino 3.4 index (green curve) during the period September 1999–October 2009. Generally, IOD peaks up during the fall season September–November, whereas enhancement of ENSO occurs during the winter period November–January. Therefore, the impacts of these two climatic episodes on the EIO winds can be expected to be maximum during the above-mentioned months. In the EIO, we have constructed the SSTA pattern (shaded) by correlating the SSTA both with DMI during September–November (Fig. 9b) and with Nino 3.4 index during November–January (Fig. 9c). To quantify the effects of wind anomalies related to the IOD and ENSO events, we have superimposed the correlation coefficients of the wind anomalies (zonal and meridional) with the climatic indices (DMI and Nino 3.4 index) as vectors over the shaded SSTA patterns (Fig. 9b, c). The response of SST to the DMI is generally strong east of 70°E in the EIO (Fig. 9b). During September–November, strong negative correlation can be noticed east of 90°E of the EIO with its peak south of the equator (Fig. 9b), while the central EIO between 60°E and

Fig. 8 Spatial patterns corresponding to the **a** first EOF mode (EOF1) explaining 50% of the variance and **c** second EOF mode (EOF2) explaining 20% of the variance of zonal wind anomalies (m s^{-1}) in the EIO domain. Monthly zonal winds during August 1999–August 2009 are used for the EOF analysis. Subplots **b**, **d** represent the time series of EOF1 and EOF2

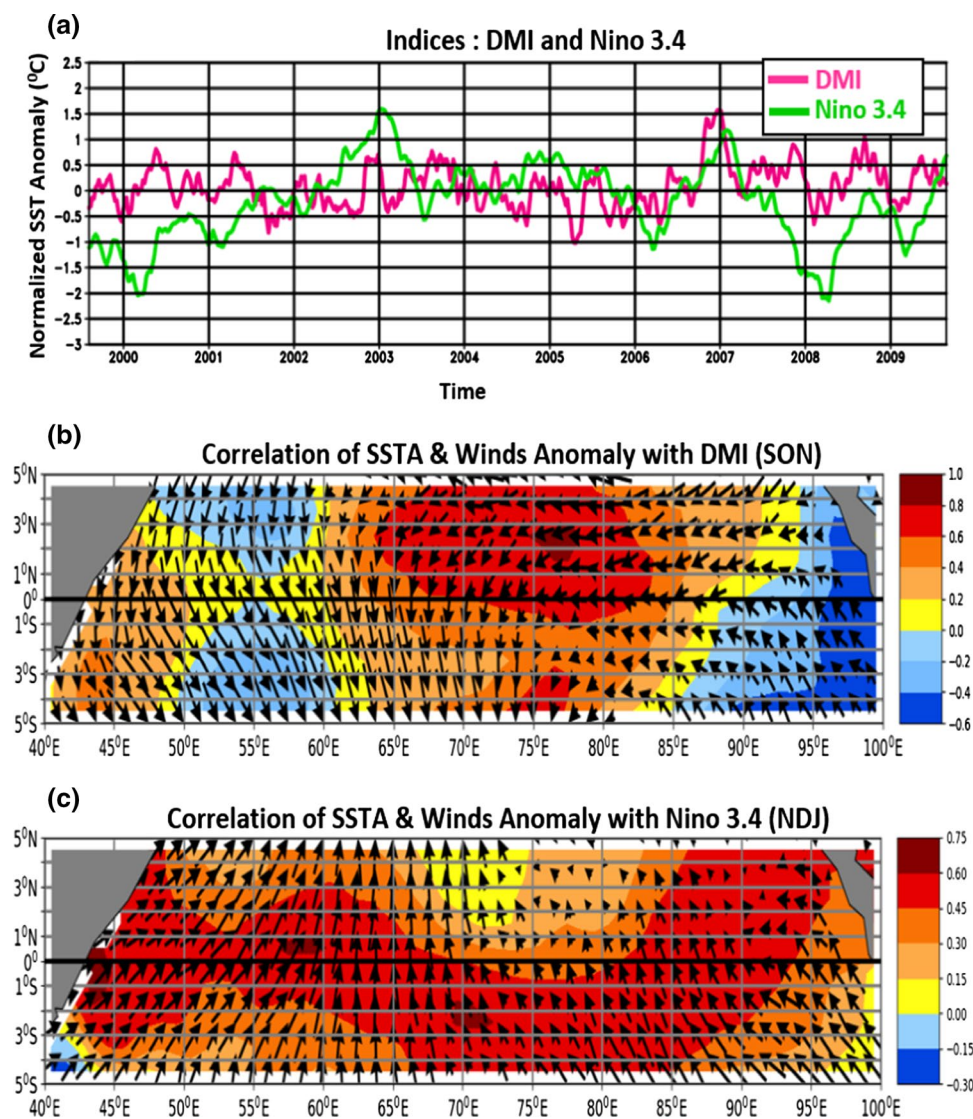


80°E exhibits a strong positive correlation north of the equator. During the PIOD event, there is a negative correlation in the eastern EIO, indicative of cooling there with substantial magnitude in the southeastern area. But the central EIO between 60°E and 80°E north of the equator shows positive correlation during PIOD, which indicates warming there. Therefore, the distribution of this strong SST gradient between the east and central areas of the EIO (Fig. 9b) suggests that such SSTA pattern can drive the occurrence of strong EIO wind anomalies during IOD events. In agreement to this, the wind variability in the EIO during the fall period September–November shows the prevalence of southeasterly anomalies east of 90°E parallel to the Sumatra coast and strong easterly anomalies north of the equator between 70°E and 90°E in the EIO domain. In contrast, the correlation of the SSTA associated with the Nino 3.4 index does not show any significant SSTA gradients in the EIO (Fig. 9c).

This observation suggests that the SSTAs in the EIO during ENSO might not be strong enough to drive the wind anomalies. However, during ENSO, there are also anomalous southeasterlies east of 70°E in the central and eastern EIO areas. This result suggests that although both IOD and ENSO events bring in anomalous southeasterlies over the EIO, the influence of IOD is stronger and affects more extensive areas of the eastern and central EIO. This attribute is precisely due to the prevalence of a strong SSTA gradient during IOD events.

The characteristics of zonal winds at different local regions of the EIO during ENSO and IOD events are also analyzed. Figure 10 shows the near-equatorial area-averaged monthly zonal winds during the inter-annual period September 1999–October 2009 (blue curve) and climatology (red curve) at various EIO regions—whole zonal stretch of the EIO region (NEIO), and western, west-central, central,

Fig. 9 **a** Dipole Mode Index (DMI) (red curve) and Nino3.4 index (green curve) during August 1999–August 2009 based on National Oceanic and Atmospheric Administration (NOAA) Optimum Interpolation Version 2 weekly SST data (Reynolds et al. 2002). The DMI is the difference in SST anomalies calculated between the western EIO (10°S–10°N and 50°–70°E) and southeastern EIO (0°–10°S and 90°–110°E). Nino 3.4 index, however, is the areal average SST anomalies calculated in the central equatorial Pacific Ocean (5°S–5°N and 170°–120°W). **b, c** Distributions of the correlations of SST anomalies (shaded) and wind anomalies (vectors) with **b** DMI (SON) and **c** Nino 3.4 index (NDJ)



and eastern (WNEIO, WCNEIO, CNEIO, and ENEIO respectively) local regions. In Sect. 3.2, for the monthly climatological zonal wind analysis also, we have considered the same areas (Fig. 4a). It turns out from Fig. 10 that the western region WNEIO shows the least inter-annual variability compared to the rest of the EIO regions. Both central and eastern areas (i.e., CNEIO and ENEIO) display significant departures from the climatology. Like the climatological zonal wind, the inter-annual variability of zonal wind also shows good correspondence between the two regions NEIO and CNEIO (Fig. 10a, d). It is evident that during certain climatic periods, westerlies strengthened, while during some other periods westerlies weakened or reversed. Those climatic periods were associated with different phases of ENSO and IOD. For instance, the most pronounced zonal wind variations at the regions NEIO (Fig. 10a), CNEIO (Fig. 10d), and ENEIO (Fig. 10e) were observed during the period August 2006–November 2006,

when the usual climatological westerlies were replaced by weak easterlies. Notably, in the CNEIO, the switchover from westerlies to easterlies persisted even for a more extended period from June 2006 to February 2007. Occurrences of the anomalous easterlies in these regions are associated with the active PIOD event during this time (Fig. 9a). Also, the westerlies strengthened abnormally during two specific periods—August 1999–April 2000 and January 2008–March 2008—in the NEIO, WCNEIO, and CNEIO regions. This can be attributed to the prevalence of high negative Niño 3.4 index during the above two periods (Fig. 9a). During both periods, the prolonged persistence of strong westerlies developed in the CNEIO region (Fig. 10d). In some years, westerlies strengthened compared to the climatological westerlies during the negative phase of DMI. For instance, during two periods—September 2001–December 2001 and May 2005–December 2005—high westerlies occurred compared to climatology in the NEIO, CNEIO, and ENEIO regions.

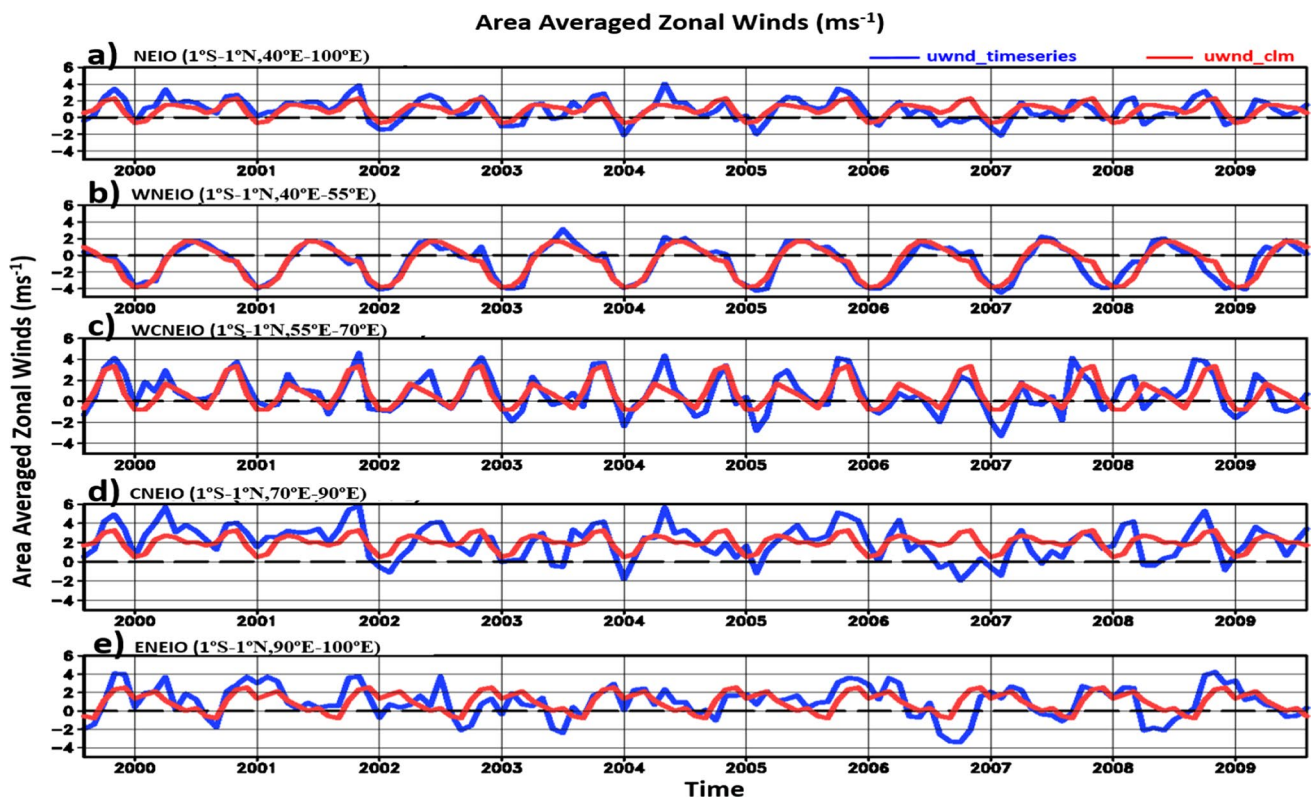


Fig. 10 a–e Near equatorial area averaged monthly zonal wind (m s^{-1}) during August 1999–August 2009 (blue curve) and its climatology (red curve) for various EIO regions. **a** whole zonal stretch of the near EIO region (NEIO) (area averaged at 1°S – 1°N , and 40°E – 100°E). **b** western near EIO region (WNEIO) (area aver-

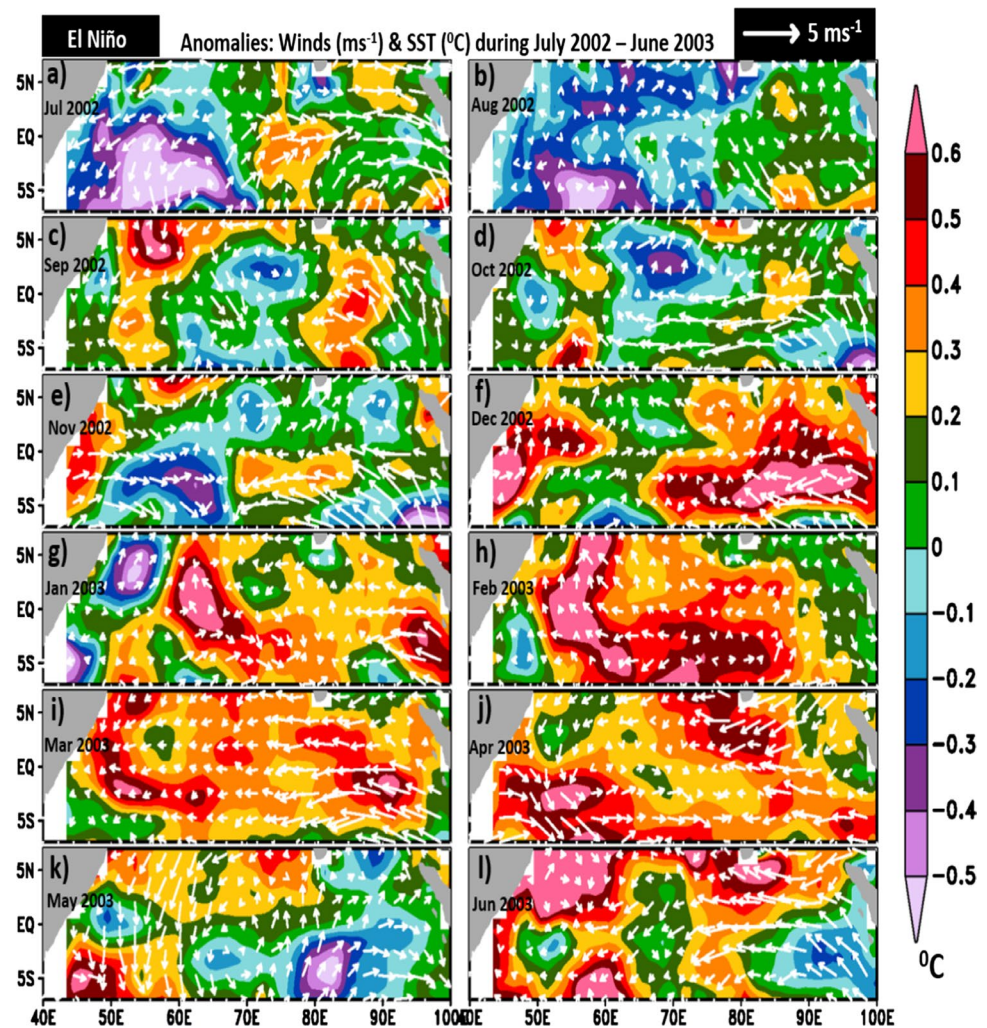
aged at 1°S – 1°N , and 40°E – 55°E). **c** west-central near EIO region (WCNEIO) (area averaged at 1°S – 1°N , and 55°E – 70°E). **d** central near EIO region (CNEIO) (area averaged at 1°S – 1°N , and 70°E – 90°E). **e** eastern near EIO region (ENEIO) (area averaged at 1°S – 1°N , and 90°E – 100°E)

Both periods coincided with the negative phases of IOD that prevailed during August 2001–December 2001 and July 2005–December 2005, respectively (Fig. 9a). Mainly, stronger zonal wind variations were observed in the CNEIO (Fig. 10d) and ENEIO (Fig. 10e) regions during the above two periods. Certain times showed a decrease in the strength of westerlies. For instance, during August 2002–May 2003, due to substantial El Niño effect, westerlies weakened in the CNEIO (Fig. 10d) and ENEIO (Fig. 10e) regions during September 2002–August 2003. In the ENEIO region, even easterlies appeared.

We have analyzed the spatiotemporal distributions of monthly wind and SST anomalies in the EIO during certain unusual ENSO and IOD events during the period September 1999–October 2009. Figure 11 shows monthly wind and SST anomalies during July 2002–June 2003 to understand the behavior of winds and SST in the EIO during El Niño event (Fig. 9a). Figure 12 shows monthly wind and SST anomalies during July 2006–June 2007 in the EIO associated with the PIOD event (Fig. 9a). Generally, the mature phase of IOD occurs during September–October (Vinayachandran et al. 2009), but not all IOD events are alike. From

Figs. 11 and 12, it can be noted that although both El Niño and PIOD events showed similar spatial wind anomalies in the EIO, month-to-month variations and strength and spatial extent during both events are much different. The strongest southeasterlies with a maximum intensity of 7 m s^{-1} occurred during PIOD event in October–November 2006 in the southeastern part of the EIO (Fig. 12d, e). But during El-Niño, southeasterlies were weaker and exhibited maximum strength of only 4 m s^{-1} during October–November 2002 (Fig. 11d, e), which subsequently weakened with the march of the annual cycle. Not only southeasterly anomalies but easterly anomalies at and near the equator east of 70°E were also stronger during PIOD compared to El Niño event. The impact of PIOD was seen over a larger area, especially anomalous winds were observed east of 60°E . But during El-Niño, relatively weak wind anomalies were found only east of 70°E . Besides, the distributions of SST anomalies were also different during the above noted El Niño and PIOD periods. During the PIOD event, the eastern EIO (east of 90°E) exhibited weak cooling one month prior (July 2006) to the appearance of the southeasterlies there (Fig. 12). With the progress of the 2006 summer season, the cooling in the

Fig. 11 a–l Monthly wind anomalies (m s^{-1}) (vectors) and SST anomalies ($^{\circ}\text{C}$) (shading) from July 2002 to June 2003 in the EIO



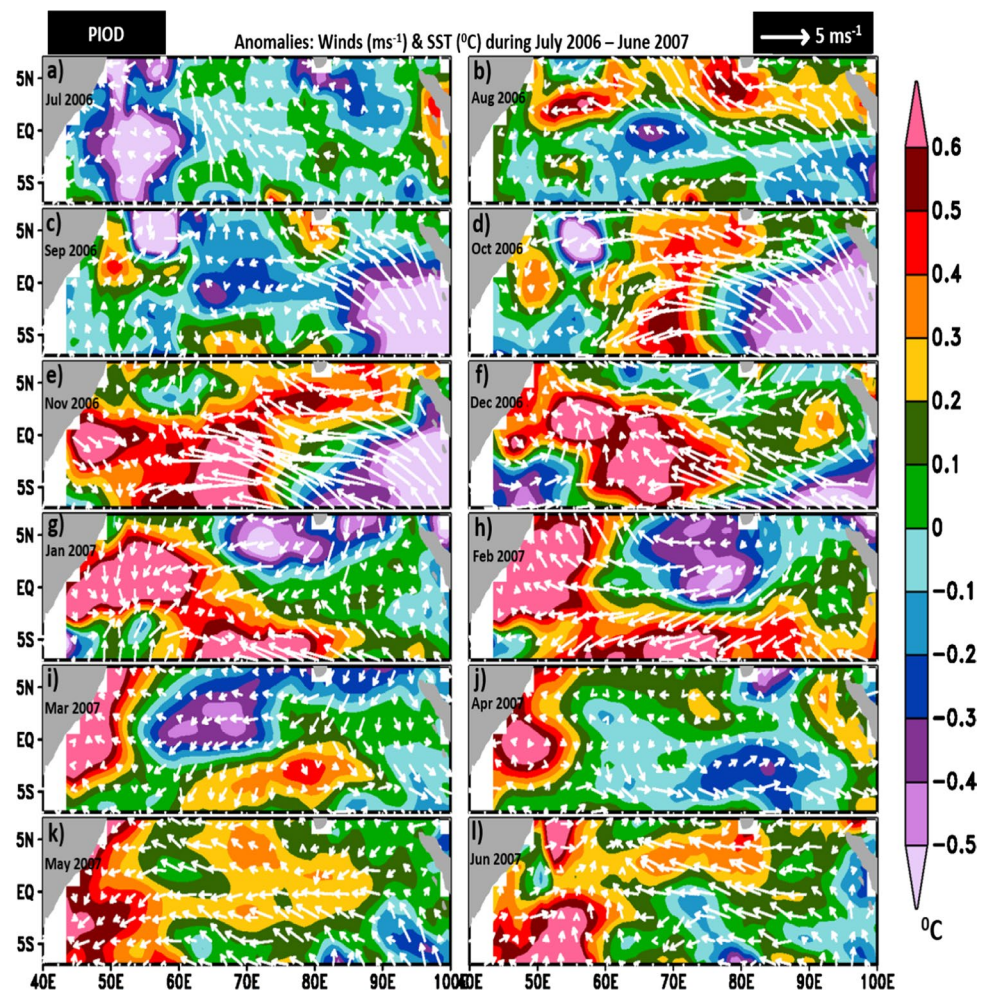
eastern EIO became even more intense. Consequently, during October–December 2006, strong east–west contrast in SSTA occurred in the EIO, with cooling in the eastern (east of 80°E) and warming in the central (60° – 80°E) regions of the EIO (Fig. 12d–f). The east–west contrast in the SST anomalies resulted in the persistence of stronger southeasterlies in most of the eastern and central EIO areas. In contrast to the PIOD during 2006–2007 (Fig. 12), the El-Niño during 2002–2003 did not show any east–west SST gradient, rather the whole EIO during this period exhibited a warming phase (Fig. 11). Figure 13 shows monthly wind and SST anomalies during August 2007–October 2008. This period reveals how the EIO winds behaved during the co-existence of La-Niña and PIOD (Fig. 9a). As a result of the combined effects of PIOD and La Niña, the EIO winds performed differently, and the abnormality persisted only for a short period. Usually, during La Niña, westerly wind anomalies are observed in the EIO. But because of the co-occurrence of La Niña with PIOD, the influence of PIOD was dominant in the EIO.

Therefore, the southeastern sector of the EIO showed southeasterlies, and near the equator east of 70°E exhibited easterlies. The most substantial southeasterly wind anomalies developed during April 2008 east of 70°E (Fig. 13i), which then weakened from June 2008 onward (Fig. 13k). Subsequently, northeasterly wind anomalies gradually replaced southeasterly wind anomalies after the vanishing of La Niña from August 2008 onwards. In the EIO, cold SST anomalies started appearing from February 2008 onwards (Fig. 13g) but intensified in April 2008 (Fig. 13i) when the southeasterlies also strengthened.

4 Summary and conclusions

Drastically different climatological winds with substantial seasonal variability occur over the monsoonal EIO compared to the equatorial Pacific and Atlantic Oceans. Seasonally varying EIO winds not only play significant

Fig. 12 a–l Monthly wind anomalies (m s^{-1}) (vectors) and SST anomalies ($^{\circ}\text{C}$) (shading) from July 2006 to June 2007 in the EIO



roles in driving the equatorial upper ocean dynamics, including the occurrence of the subsurface EUC but also influence the air–sea interactive processes in the Indian Ocean region. Many previous studies have only attempted to understand the broad-scale characteristics of the EIO winds. In the present study, using satellite-sensed high-resolution ($0.25^{\circ} \times 0.25^{\circ}$) monthly winds covering the period September 1999–October 2009, we have focused on understanding the salient features of the seasonal and inter-annual variabilities of surface winds occurring at various dynamically significant regions (west, west-central, central, and east) of the EIO. Besides winds, we have also used monthly Sea Level Pressure as well as monthly SST datasets during the period September 1999–October 2009. The Sea Level Pressure data are useful in understanding the role of one of the forcings for maintaining the EIO winds, while the SST data help in discerning the ocean dynamics associated with the variabilities of the EIO winds. In summary, the salient features of the EIO winds based on this study are drawn below.

- *Annual mean pattern*

In a significant portion of the EIO east of 60°E , the climatological annual mean surface winds are westerlies with increasing strength up to 90°E and peak westerlies in the east-central area between 80°E and 90°E , whereas the annual mean surface wind pattern shows easterlies in the equatorial Pacific and Atlantic Oceans. But west of 60°E of the EIO, the annual mean winds are either southerlies or southeasterlies with the maximum in the Somalia region. The coverage of high wind steadiness in the westerlies bounded region east of 70°E of the EIO shows there the occurrences of strong summer monsoon winds during May–September in one direction and relatively weak winter monsoon winds during December–March in the opposite direction. West of 50°E of the EIO, winds are highly variable both in magnitude and direction in the Northern Hemisphere due to low wind steadiness compared to the Southern Hemisphere where with high wind steadiness. The annual mean pattern of the EIO winds mainly shows the distributions of southerlies and westerlies. Therefore, both the migrations and the fluctuations

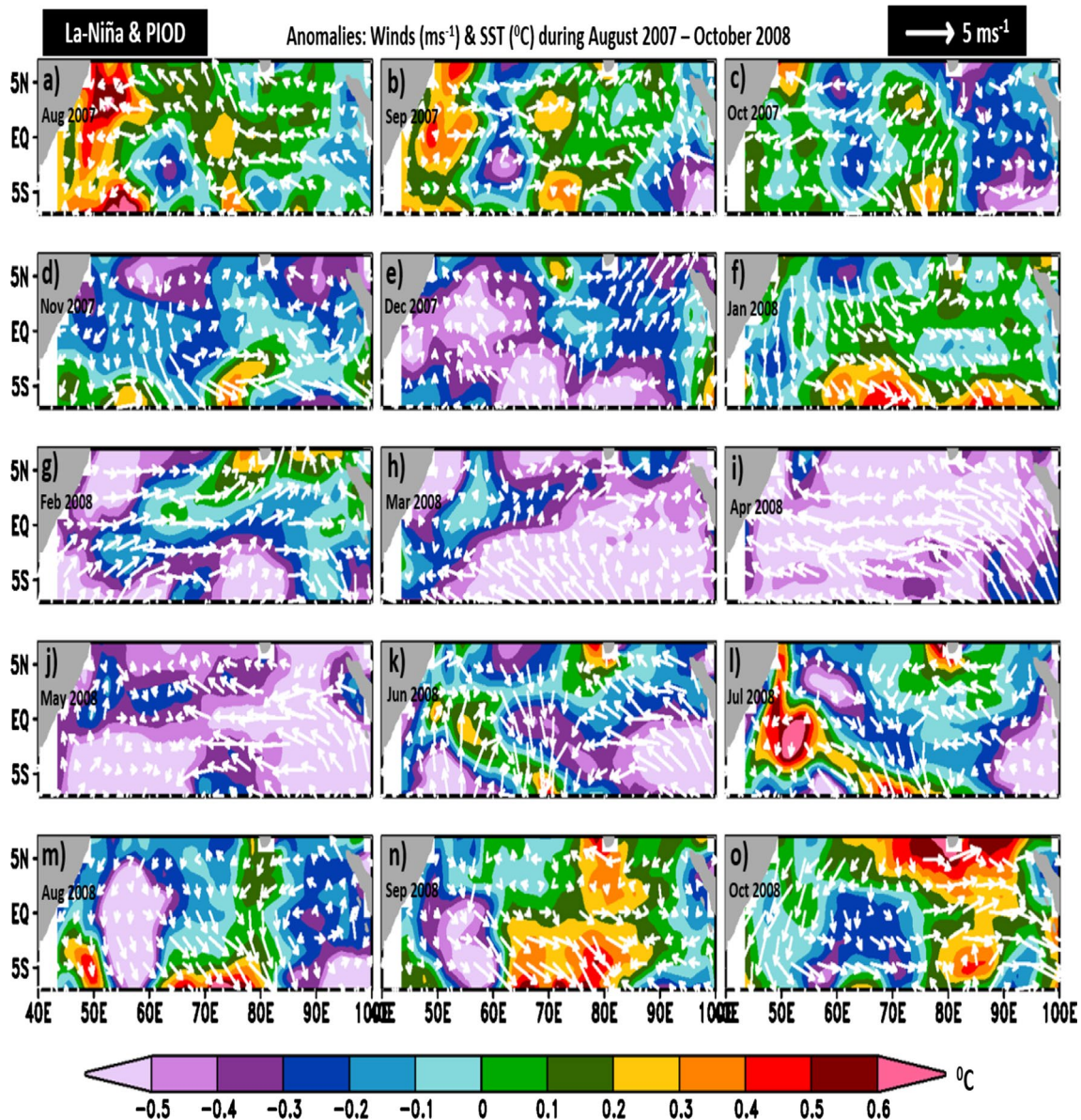


Fig. 13 a–o Monthly wind anomalies (m s^{-1}) (vectors) and SST anomalies ($^{\circ}\text{C}$) (shading) from August 2007 to October 2008 in the EIO

of equatorial southerlies and westerlies play crucial roles for any remarkable wind variations, such as seasonal, intra-seasonal, and inter-annual, occurring in the EIO.

- *Seasonal variability*

Seasonal variability of wind speed is high in two prime areas located north of the equator—west of 60°E and the east-central part between 80°E and 90°E . But, near the equator, east of 80°E in the Southern Hemisphere shows low seasonal wind speed variability. During the four cardinal seasons (i.e., SW and NE monsoons, and transitions between the monsoons), wind variability is different at various local regions of the EIO. Also, the four seasons occur during different months at the various local areas.

Though seasonal wind variations are alike in the western and west-central EIO regions, magnitude-wise weaker winds arise in the west-central area compared to the western part. In the central part of the EIO, weaker winds occur close to the equator, especially within 1°S – 1°N , during SW and NE monsoons, whereas high winds blow over this region during monsoon transition periods.

In the western EIO, SW and NE monsoons are longer with stronger winds, but both seasons are shorter with weaker winds in the eastern EIO. Between 40°E and 55°E of the western EIO, NE monsoon winds occur during December–March with strong winds during January–February. But in the eastern EIO east of 90°E , NE mon-

soon winds are weaker and remain for a shorter period during January–February. In the central EIO, on the other hand, NE monsoon occurs during December–February with the maximum winds within 78°E–90°E during January–February. A conspicuous feature during March is the development of the equatorial westerlies east of 65°E and within 1°N–3°S. During April, the weakest winds of the annual cycle occur everywhere in the EIO except the central part where well-developed strong westerlies blow with its core near the equator and diminishing strength on either side of the equator. In the western EIO west of 55°E, summer monsoon winds blow over an extended period May–October, with the intensity increasing westward of 55°E with peak winds during June–August. In the west-central and central EIO regions, SW monsoon winds occur during May–September. But in the eastern EIO, weak summer monsoon winds arise during June–September with the maximum intensity during July–August. In the central EIO, winds occurring during fall (October–November) and spring (April–May) transition periods are stronger compared to SW and NE monsoon winds.

The meridional and zonal wind components exhibit striking characteristics in their occurrence, strengthening, and weakening at various local regions of the EIO. At the western and eastern boundaries of the EIO, the seasonal variability of winds is primarily determined by the meridional wind as this component becomes the dominant one there as a result of the influence of mountains, land–sea contrast, and beta effect. Throughout the year, meridional EIO winds are weak in the eastern basin compared to its western counterpart. In the EIO, near the equator, the annual harmonic of the meridional wind is more significant than the semi-annual harmonic, especially in the western part of the EIO. During monsoons, the winds show a dominant meridional component near the equator, which is southward during NE monsoon and northward during SW monsoon, particularly at the western boundary. Also, during the peak time of NE (January–February) and SW (June–August) monsoons, meridional winds show a zonal gradient from west to east. Close to the equator, the annual cycles of meridional wind in the whole EIO and west-central part of the EIO are much similar even amplitude-wise also. Another characteristic is that west of 60°E of the EIO, the switchover between southerlies and northerlies mostly co-occurs throughout the latitudinal stretch 5°S–5°N.

In the EIO, except the western and eastern boundary regions, the zonal wind component is a significant contributor to the total wind field. The zonal wind regime shows that westerlies and easterlies occur during different periods at various local areas of the EIO. In general,

in the EIO, westerlies are stronger compared to easterlies. Stronger westerlies occur during peak SW monsoon (June–August) in the western EIO and during spring (April–May) and fall (October–November) transition periods in the central and east-central parts of the EIO. But strong easterlies occur during peak winter (January–February) in the western EIO. In the majority of the EIO east of 55°E, well-organized westerlies blow during fall and spring seasons, with the maximum westerlies in the central ocean within 60°E–90°E. During fall, westerlies are stronger in October; whereas during spring strong westerlies occur in May, especially entire EIO north of the equator and southern latitudes close to the equator. While comparing the transition periods, strong westerlies of the EIO arise during fall. After May, the westerlies continue to be present in the entire EIO north of the equator during SW monsoon season (June–September), with peak strength in July and weakening in September. During June–August, maximum westerlies occur in two areas—western and east-central—of the EIO. But during NE monsoon (December–February), easterlies cover the entire EIO north of the equator, with peak easterlies west of 80°E during January–February. In this season, the majority of the EIO west of 55°E shows easterlies during December–March, with high intensity during January–February and weakening in March. Near to the equator, the eastern EIO shows westerlies most of the year except for the occurrence of weak easterlies during the SW monsoon period (June–September). But the near-equator western part of the EIO shows strong westerlies during SW monsoon and strong easterlies during NE monsoon. Also, close to the equator, the zonal wind variabilities occurring in the central EIO is a decisive factor in understanding the zonal wind variations of the whole EIO region. The zonal wind regime of the near-equator of the EIO shows significant contributions both from the annual and semi-annual harmonics. Like the meridional wind, the amplitude of the annual harmonic of zonal wind is also high near the western boundary of the EIO due to the occurrence of intense reversing monsoon winds off Somalia. The zonal wind also shows relatively smaller annual harmonic component peaks in the central EIO near 80°E and in the eastern boundary near 96°E, which can be attributed to the extension of monsoon winds southward from south of Sri Lanka and along the Indonesian coast, respectively. In contrast, the semi-annual harmonic component of the near-equator EIO zonal wind shows westerlies during spring and fall and easterlies during SW and NE monsoons. Also, this component exhibits a simple structure with a single maximum located in the central ocean between 60°E and 80°E.

The present study reveals that the dynamics of the zonal winds in the near-equator region (between 1°S and 1°N) of the EIO is mainly controlled by the zonal Sea Level Pressure gradient and momentum advection fields. The annual harmonics of both these fields exhibit opposite accelerations during November–March and April–October. However, the semi-annual components of both the zonal Sea Level Pressure gradient and momentum advection exhibit strong but opposite accelerations throughout the year between 45°E and 60°E of the western EIO. That is, specifically in this longitudinal belt of the western EIO, during both NE and SW monsoons, the semi-annual component shows easterly acceleration of momentum advection and westerly acceleration of zonal Sea Level Pressure gradient. Also, during the transition periods, in this region, the semi-annual component of both the fields displays opposite accelerations. Consequently, in the western part of the EIO, the opposite accelerations of the semi-annual harmonic components of both the fields become responsible for the weakness of zonal winds, despite each of them having the most substantial magnitude there. However, unlike this, in the central part of the EIO between 60°E and 80°E, the semi-annual component of the momentum advection and the zonal Sea Level Pressure gradient, although weak, displays synonymous accelerations throughout the year, causing the occurrence of strong zonal winds in this longitudinal belt.

- *Inter-annual variability*

The inter-annual variability of winds in the EIO during the period from August 1999 to August 2009, in the light of climatic events like ENSO and IOD, is also studied. The ENSO and IOD exhibit different impacts of winds in the EIO, which primarily affect the central and eastern parts of the EIO. In comparison to the meridional wind, the zonal wind has showcased stronger inter-annual variability. The EOF analysis shows that the first two modes dominate the inter-annual variability of zonal winds in the EIO. The first mode (EOF1) explains 50% and the second mode (EOF2) 20% of the total variance of the zonal winds in the EIO. The spatial pattern corresponding to EOF1 resembles the normal zonal wind distribution occurring in the EIO during the monsoon transition periods of spring and fall. However, EOF2 describes the variability of the zonal winds during the SW monsoon season. Though the EOF analysis has demonstrated the dominant modes of the inter-annual variability of zonal winds in the EIO, it could not precisely capture the IOD and ENSO effects on the EIO winds. Correlations of the winds and SST anomalies with the DMI (September–November) have revealed that the IOD events affect the patterns of winds and SST in the EIO. The SST anomaly and the DMI are negatively correlated east of 90°E of

the eastern EIO; while both are positively correlated in the central part of the EIO between 60°E and 80°E, with high amplitude north of the equator. Distribution of the correlation pattern like this clarifies that during the PIOD event, there is a cooling taking place in the eastern EIO, whereas warming in the central EIO. Consequently, the development of strong SST gradient like this drives strong anomalous easterly winds along the equator in the east-central region between 70°E and 90°E north of the equator, and unusual southeasterly winds parallel to the Sumatra coast. The ENSO events also show anomalous southeasterlies in the eastern EIO, especially south of the equator, but the impact induced by these winds in the ocean is comparatively weaker than the IOD event.

During the periods of unusual climatic events such as IOD, ENSO or the co-occurrence of both, the most substantial zonal wind anomalies occur in the eastern and central parts of the EIO, whereas weak anomalies develop in the western EIO. Herein, we have also examined the spatiotemporal variations of winds during three events that occurred during the periods 2006–2007, 2002–2003, and 2007–2008. Selection of these years has facilitated to analyze the characteristics of winds in the EIO separately during PIOD, El-Niño, and during co-occurrence of La-Niña and PIOD events. The analysis has revealed that both El-Niño and PIOD events showed the same kind of spatial patterns of wind anomalies, but their month to month variations, spatial extensions and intensities are different. Even though both events resulted in anomalous southeasterly winds in the EIO, for PIOD the effect was stronger and was seen on a larger area, which is also following a previous study (Gnanaseelan et al. 2012). Anomalous strong southeasterly winds occupied east of 60°E during PIOD, while during El-Niño unusual weak southeasterly winds held east of 70°E. The signatures of PIOD during 2006 were seen even 2 months before the occurrence of the event, but in the case of El-Niño, it was different. During El-Niño, weak anomalous southeasterlies were observed only 1 month after the onset of the event. As far as the latitudinal distribution of zonal wind is concerned, the most active anomalous easterlies were seen in the central and eastern regions within the latitudinal stretch 5°S–2°N during PIOD of 2006–2007.

The present study on the seasonal and inter-annual variability of EIO winds has shed light on which oceanic areas of the EIO basin are so vital for understanding the upper ocean dynamics and circulation features. The seasonally varying monsoon winds of the EIO force the surface and subsurface currents in this region. Both the surface and subsurface zonal currents at the EIO play integral roles in modulating the surface and subsurface features. For example, the surface WJs occurring during monsoon transition seasons are intimately linked to modulating the heat content in the eastern

EIO warm pool region by transporting upper ocean mass and heat along the equator from west to east. The WJs are driven by the equatorial westerlies, while the subsurface Equatorial Undercurrent (EUC) of the thermocline region during winter and spring seasons are generated by the eastward pressure gradient force caused primarily by the equatorial easterly winds. Therefore, as we have shown in this study, knowledge of the wind variations occurring over different local areas of the EIO region can help in understanding the variabilities of the surface and subsurface circulation features of the EIO.

Acknowledgements This research work is a part of the two climate change-related research projects funded by the organizations CSIR-National Institute of Science Communication and Information Resources (CSIR-NISCAIR), New Delhi, and Department of Science and Technology, New Delhi. We also much appreciate the comments from anonymous reviewers, and the suggestions and encouragement from the Editor of the journal, which led to improving the article substantially.

References

- Balmaseda MA, Mogensen K, Weaver AT (2013) Evaluation of the ECMWF ocean reanalysis system ORAS4. *Q J R Meteorol Soc* 139(674):1132–1161
- Chakraborty A, Nanjundiah RS, Srinivasan J (2009) Impact of African orography and the Indian summer monsoon on the low-level Somali jet. *Int J Climatol* 29(7):983–992
- Chen G, Han W, Li Y, Wang D, McPhaden MJ (2015) Seasonal-to-Interannual time-scale dynamics of the Equatorial Undercurrent in the Indian Ocean. *J Phys Oceanogr* 45(6):1532–1553
- Chen G, Han W, Li Y, Wang D (2016) Interannual variability of equatorial eastern Indian ocean upwelling: local versus remote forcing. *J Phys Oceanogr* 46(3):789–807. <https://doi.org/10.1175/JPO-D-15-0117.1>
- Clarke AJ, Liu X (1993) Observations and dynamics of semiannual and annual sea levels near the eastern equatorial Indian ocean boundary. *J Phys Oceanogr* 23(2):386–399
- Findlater J (1969) A major low-level air current near the Indian Ocean during the northern summer. *Q J R Meteorol Soc* 95:362–380
- Francis PA, Gadgil S (2009) The aberrant behavior of the Indian monsoon in June 2009. *Curr Sci* 97(9):1291–1295
- Freilich M (2000) SeaWinds: algorithm theoretical basis document. NASA ATBD-SWS-01
- Gadgil S, Vinayachandran PN, Francis PA (2004) Extremes of the Indian summer monsoon rainfall, ENSO and the equatorial Indian Ocean Oscillation. *Geophys Res Lett* 31:L12213. <https://doi.org/10.1029/2004GL019733>
- Gill AE (1980) Some simple solutions for heat-induced tropical circulation. *Q J R Meteorol Soc* 106(449):447–462. <https://doi.org/10.1002/qj.49710644905>
- Gnanaseelan C, Deshpande A, McPhaden MJ (2012) Impact of Indian Ocean dipole and El Niño/Southern Oscillation wind-forcing on the Wyrтки jets. *J Geophys Res* 117:C08005. <https://doi.org/10.1029/2012JC007918>
- Han W, Webster PJ (2002) Forcing mechanisms of sea level interannual variability in the Bay of Bengal. *J Phys Oceanogr* 32(1):216–239
- Hastenrath S, Nicklis A, Greischar L (1993) Atmospheric-hydrospheric mechanisms of climate anomalies in the western equatorial Indian Ocean. *J Geophys Res* 98:20219. <https://doi.org/10.1029/93JC02330>
- Hastenrath S, Polzin D (2004) Dynamics of the surface wind field over the equatorial Indian Ocean. *Quat J R Meteorol Soc* 130(597):503–517. <https://doi.org/10.1256/qj.03.79>
- Huang B, Kinter JL III (2002) Interannual variability in the tropical Indian Ocean. *J Geophys Res* 107:3199. <https://doi.org/10.1029/2001JC001278>
- Iskandar I, Mardiansyah W, Masumoto Y, Yamagata T (2005) Intraseasonal Kelvin waves along the southern coast of Sumatra and Java. *J Geophys Res Ocean* 110(4):1–12. <https://doi.org/10.1029/2004JC002508>
- Iskandar I, Masumoto Y, Mizuno K (2009) Subsurface equatorial zonal current in the eastern Indian Ocean. *J Geophys Res: Ocean* 114(C06005):1–12. <https://doi.org/10.1029/2008JC005118>
- Jakubasukas ME, Legates DR, Kastens JH (2001) Harmonic analysis of time-series AVHRR NDVI data. *Photogramm Eng Remote Sens* 67:461–470
- Jenkins GM, Watts DG (1968) Spectral analysis and its applications (5th printing of the 1968 edition). Holden-Day, San Francisco, p 525
- Knox RA (1976) On a long series of measurements of Indian Ocean equatorial currents near Addu Atoll. *Deep-Sea Res Oceanogr Abstr.* [https://doi.org/10.1016/0011-7471\(76\)91325-5](https://doi.org/10.1016/0011-7471(76)91325-5)
- Krishnamurti TN, Molinari J, Pan HL (1976) Numerical simulation of the Somali Jet. *J Atmos Sci* 33:2350–2362
- Lindzen RS, Nigam S (1987) On the role of sea surface temperature gradients in forcing low-level winds and convergence in the tropics. *J Atmos Sci* 44:2418–2436
- Lungu T (2001) QuikSCAT Science data product user's manual, version 2.2, JPL document D-18053. Jet Propulsion Laboratory, Pasadena
- McCreary JP, Kundu PK, Molinari RL (1993) A numerical investigation of dynamics, thermodynamics and mixed-layer processes in the Indian Ocean. *Prog Oceanogr.* [https://doi.org/10.1016/0079-6611\(93\)90002-U](https://doi.org/10.1016/0079-6611(93)90002-U)
- McCreary JP, Han W, Shankar D, Shetye SR (1996) Dynamics of the East India coastal current: 2 numerical solutions. *J Geophys Res* 101:13993–14010
- Murtugudde R, Busalachi A (1999) Interannual variability of the dynamics and thermodynamics of the tropical Indian Ocean. *J Clim* 12:2300–2326
- National Geophysical Data Center (2006) 2-minute gridded global relief data (ETOPO2) v2. Natl Geophys Data Center NOAA. <https://doi.org/10.7289/V5J1012Q>
- Okumura Y, Xie SP (2004) Interaction of the Atlantic equatorial cold tongue and African monsoon. *J Clim* 17:3588–3601
- Onogi K, Tsutsui J, Koide H, Sakamoto M, Kobayashi S, Hatsushika H, Matsumoto T, Yamazaki N, Kamahori H, Takahashi K, Kado-kura S (2007) The JRA-25 reanalysis. *J Meteorol Soc Jpn Ser II* 85(3):369–432
- Potemra JT, Luther ME, O'Brien JJ (1991) The seasonal circulation of the upper ocean in the Bay of Bengal. *J Geophys Res* 96(91):12667–12683. <https://doi.org/10.1029/91JC01045>
- Rao RR, Girish Kumar MS, Ravichandran M, Rao AR, Gopalakrishna VV, Thadathil P (2010) Interannual variability of Kelvin wave propagation in the wave guides of the equatorial Indian Ocean, the coastal Bay of Bengal and the Southeastern Arabian Sea during 1993–2006. *Deep Sea Res Part 1*(57):1–13
- Reynolds RW, Rayner NA, Smith TM, Stokes DC, Wang W (2002) An improved in situ and satellite SST analysis for climate. *J Clim* 15(13):1609–1625. [https://doi.org/10.1175/1520-0442\(2002\)015<1609:AIISAS2.0.CO;2](https://doi.org/10.1175/1520-0442(2002)015<1609:AIISAS2.0.CO;2)
- Saji NH, Goswami BN, Vinayachandran PN, Yamagata T (1999) A dipole mode in the tropical Indian Ocean. *Nature* 401(6751):360

- Schott FA, Dengler M, Schoenefeldt R (2002) The shallow overturning circulation of the Indian Ocean. *Prog Oceanogr* 53(1):57–103. [https://doi.org/10.1016/S0079-6611\(02\)00039-3](https://doi.org/10.1016/S0079-6611(02)00039-3)
- Schott FA, Xie SP, McCreary JP Jr (2009) Indian Ocean circulation and climate variability. *Rev Geophys* 47(2007):1–46. <https://doi.org/10.1029/2007RG000245>
- Senan R, Sengupta D, Goswami BN (2003) Intraseasonal “monsoon jets” in the equatorial Indian Ocean. *Geophys Res Lett* 30(14):1–4. <https://doi.org/10.1029/2003GL017583>
- Shaji C, Iizuka S, Matsuura T (2003) Seasonal variability of near-surface heat budget of selected oceanic areas in the North Tropical Indian Ocean. *J Oceanogr* 59(1):87–103. <https://doi.org/10.1023/A:1022872524758>
- Shankar D, Vinayachandran PN, Unnikrishnan AS (2002) The monsoon currents in the north Indian Ocean. *Prog Oceanogr* 52(1):63–120. [https://doi.org/10.1016/S0079-6611\(02\)00024-1](https://doi.org/10.1016/S0079-6611(02)00024-1)
- Singer IA (1967) Steadiness of the wind. *J Appl Meteorol* 6(6):1033–1038
- Tsai PTH, Obrien JJ, Luther ME (1992) The 26-day oscillation observed in the satellite sea-surface temperature-measurements in the Equatorial Western Indian-Ocean. *J Geophys Res Oceans* 97:9605–9618
- Vinayachandran PN, Iizuka S, Yamagata T (2002) Indian Ocean dipole mode events in an ocean general circulation model. *Deep Sea Res Part II Top Stud Oceanogr* 49(7–8):1573–1596. [https://doi.org/10.1016/S0967-0645\(01\)00157-6](https://doi.org/10.1016/S0967-0645(01)00157-6)
- Vinayachandran PN, Francis PA, Rao SA (2009) Indian Ocean dipole: processes and impacts. *Current trends in science (Platinum Jubilee Special Publication)*. Indian Academy of Sciences, Sadashivnagar, pp 569–589
- Webster PJ (1972) Response of the tropical atmosphere to local. *Steady Forcing Mon Weather Rev* 1000(7):518–541
- Yamagata T, Mizuno K et al (1996) Seasonal variations in the equatorial Indian Ocean and their impact on the Lombok throughflow. *J Geophys Res* 101:12465–12474
- Yu L, O’Brien JJ, Yang J (1991) On the remote forcing of the circulation in the Bay of Bengal. *J Geophys Res* 96(CII):20449–20454. <https://doi.org/10.1029/91JC02424>

Publisher’s Note Springer Nature remains neutral with regard to jurisdictional claims in published maps and institutional affiliations.